

Structural Fatigue Evaluation of Turbine B2 Block Island Wind Farm

BSEE Project Report
DRAFT

Contract Number 140E0119C0003

Nasim Partovi Mehr¹, John DeFrancisci¹, Mohsen Minaeijavid¹, Babak Moaveni², Dan Kuchma², Eric M. Hines³

¹ *Graduate Research Assistant*

² *Professor*

³ *Professor of the Practice*

Department of Civil and Environmental Engineering, Tufts University, Medford, MA 02155

May 2023

Contents

| | | |
|------------|--|----|
| 1 | Executive Summary | 3 |
| 2 | Introduction..... | 3 |
| 3 | Fatigue assessment using strain gauges | 3 |
| 3.1 | Stress and Bending moment at instrumented section | 4 |
| 3.2 | Stress at non-instrumented section | 5 |
| 3.3 | Rainflow Counting | 6 |
| 3.4 | Fatigue damage during the monitoring period and estimating the remaining lifetime. ... | 7 |
| 4 | The B2 Offshore Wind Turbine and its Monitoring System | 11 |
| 4.1 | Block Island Wind Farm | 11 |
| 4.2 | Monitoring System of Strain Gauges | 11 |
| 4.3 | Dataset Selection | 12 |
| 5 | Experimental Results | 13 |
| 5.1 | Fatigue Assessment of the BIWF-B2 Tower | 13 |
| 5.1.1 | Sources of Fatigue Damage in Tower..... | 16 |
| 5.1.2 | Time Series Investigation | 20 |
| 5.2 | Fatigue Assessment of the BIWF-B2 Jacket | 21 |
| 5.2.1 | Stress estimation at jacket joints..... | 21 |
| 5.2.2 | Damage and Fatigue life estimation | 24 |
| 5.2.3 | Effects of environmental/operational conditions on damage..... | 27 |
| 6 | Conclusions..... | 32 |
| 7 | Acknowledgments..... | 33 |
| 8 | References..... | 33 |
| | Appendix A..... | 35 |
| | Appendix B..... | 36 |
| | Appendix C | 41 |

1 Executive Summary

Offshore wind turbine (OWT) support structures are subjected to cyclic dynamic loads from wind, waves, etc. during their lifetime. Because of this repeated cyclic loading, the fatigue limit state can be a dominant case for the design of the support structures of OWTs. This report summarizes the structural fatigue behavior of Turbine B2 within the Block Island Wind Farm which has been instrumented with accelerometers and strain gauges and monitored for at least one year under this research grant (Hines et al., 2023). This report provides the fatigue assessment process in Section 3. The studied B2 turbine and its instrumentation is discussed in Section 4. Section 5 investigates the experimental fatigue life results in two subsections: Section 5.1 for the tower and Section 5.2 for the jacket support structure.

2 Introduction

The load cases for offshore wind support structure design are established in “IEC 61400 Wind energy generation systems – Part 3-1: Design requirements for fixed offshore wind turbines” (IEC, 2019). The fatigue limit state is often a major focus for designers and researchers (Augustyn et al., 2021; Ding et al., 2022; Joey et al., 2020; Renqiang et al., 2021).

These load cases include operational fatigue loads (DLC 1.2), special conditions (i.e., DLC 2.4, DLC 3.1, DLC 4.1), and parked conditions (i.e., DLC 6.4).

This report has two primary aims. First, an in-depth analysis of tower fatigue investigates potential causes of fatigue damage. While the section at the base of the tower was instrumented with strain gages, it is known not to be a fatigue-critical part of the structural system. However, the behavior at the tower base provides a useful framework for understanding fatigue demands. Second, strain gauge measurements are used to calculate the thrust at hub-height level and then a SAP2000 finite element (FE) model of the turbine is used to provide an estimate of the jacket joints stress due to the thrust. Finally, fatigue damage of the jacket is assessed.

3 Fatigue assessment using strain gauges

The four strain gauges (SG) installed at the base of the tower provide the primary measurements for fatigue assessments in this report. Information related to the installation and data from these strain gauges can be found in section 4.2. The strain gauge information is used to develop two separate representations of fatigue demand:

1. Calculation of stresses at the strain gauge locations.
2. Calculation of tower base-moments and hub-height thrusts based on strains that can then be used as inputs for a finite element model in order to estimate the fatigue demands on the jacket foundation structure.

The details of Item 2 above are discussed in Sections 3.1—3.3.

3.1 Stress and Bending moment at instrumented section

Tower fatigue was evaluated at four SG locations of the instrumented section which is 0.7 m above the bolt ring at the tower base. Stress at the SG locations (σ_i), is calculated based on the axial SG measurements (ϵ_i) as shown in Equation 1.

$$\sigma_i = E \epsilon_i \quad \text{Equation 1}$$

where E is the Young's modulus of the steel, assumed to be 200 GPa.

As the SG sensors measure the variation from the initial stress state of the structure, they require calibration prior to their use in the previous equation. The calibration process is described in report M2.4 of this project. The bending moments in two perpendicular directions in the global coordinates (u,v), as shown in Figure 1, can then be used to determine the bending moments in the fore-aft (FA) and side-side(SS) directions. The nacelle orientation defines the FA direction and SS is perpendicular to it. We calculate moments in FA (M_{FA}) and SS (M_{SS}) directions as follows:

$$\begin{aligned} M_{FA} &= M_u \cos \theta - M_v \sin \theta \\ M_{SS} &= M_u \sin \theta + M_v \cos \theta \end{aligned} \quad \text{Equation 2}$$

where M_u and M_v are the bending moments in u and v directions, and θ is the yaw angle starting at magnetic North and is positive clockwise.

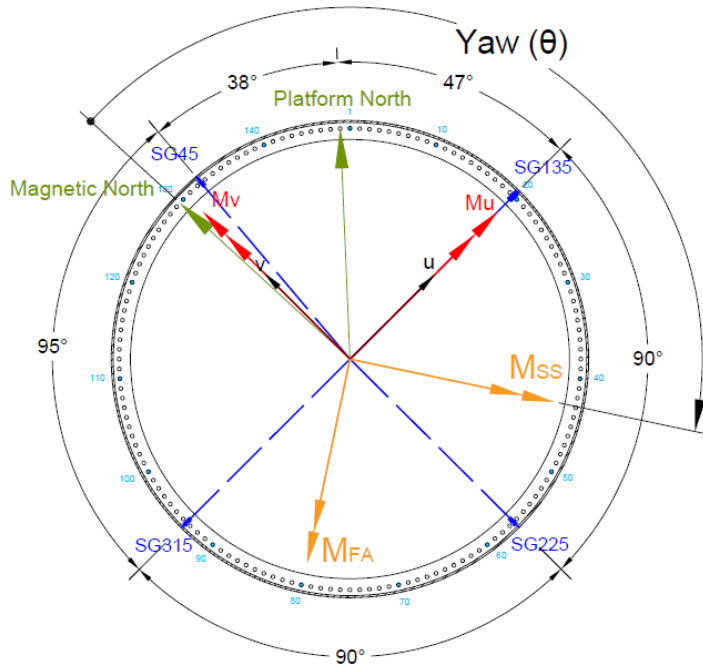


Figure 1. Strain gauge orientation and North direction.

Note that due to the slight offset of SG45 from Magnetic North, principal axes are defined as M_u along SG135 and SG315 as shown in Figure 1. Positive M_v is then defined as 90 degrees counterclockwise from positive M_u , which situates M_v between Magnetic North and SG45. The light blue numbers, beginning with the number 1 positioned slightly clockwise from Platform North, represent bolt numbers. During installation, the locations of SGs were noted according to

bolt number as shown in Figure 2. During installation, the SGs were accidentally offset approximately 90° counter-clockwise from their compass designation with respect to Platform North, which occurs at Bolt 148 as shown in Figure 1 and Figure 2. While these designations are not ideal, they have been maintained in this report for the purpose of consistency with past analyses and reports.

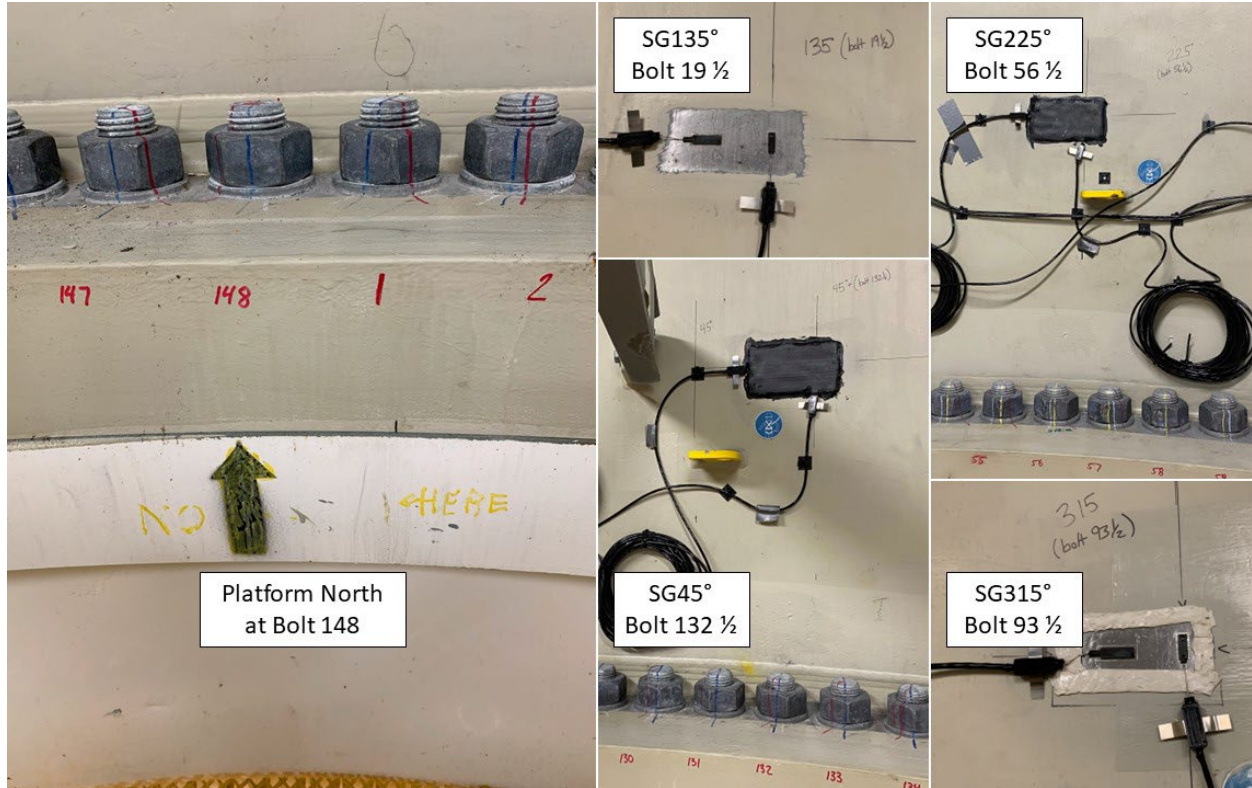


Figure 2. Turbine B2 strain gauge locations according to Bolt Number.

3.2 Stress at non-instrumented section

Jacket fatigue was evaluated based on the stresses obtained from a SAP2000 FE model of the support structure for Turbine B2. The thrust force was calculated, as shown in Equation 4, from the bending moments at the instrumented section and applied to the FE model. The resulting stresses on any point of the jacket foundation were determined via static analysis of the turbine structure. As part of the calibration process, the resulting self-weight moment of the RNA at the instrumented location is calculated as 17.72 MN m according to Equation 3.

$$(430t) \left(9.81 \frac{\text{m}}{\text{s}^2} \right) (4.2\text{m}) = 17.72 \text{ MNm} \quad \text{Equation 3}$$

$$\text{Thrust} = \frac{M_{FA} + 17.72}{82.85} \text{ (MN)} \quad \text{Equation 4}$$

where 82.85 m is the vertical distance between the rotor nacelle assembly (RNA) center of mass and the strain gauges near the tower base.

Obtaining the thrust for each yaw angle, a static load can be applied to the FE model for each time-step, resulting in an estimate for the stress at any jacket node. Additional descriptions of the method used to determine jacket stresses is provided in Section 5.3.

3.3 Rainflow Counting

Referring to IEC 61400-3-1 rainflow cycle counting is a conservative method of counting cycles that is often used for fatigue design and assessment. In addition to rainflow counting, the IEC standard also allows mean cycle crossing methods to be used, however, rainflow cycle counting appears to be a commonly used method in the wind industry (Pacheco et al., 2022). Therefore, rainflow cycle counting method was selected for this report.

Rainflow cycle counting is defined in ASTM E1049-85 Standard Practices for Cycle Counting in Fatigue Analysis (ASTM-E1049-85, 2017). MATLAB also has a rainflow cycle counting function built into it. This function uses the same algorithm defined in ASTM E1049-85. Figure 3, taken from MATLAB documentation, shows the overall process behind rainflow counting. The result of rainflow counting is a series of full and half cycle counts associated with a stress cycle range and a mean stress. For a more detailed discussion of this process please see Appendix C.

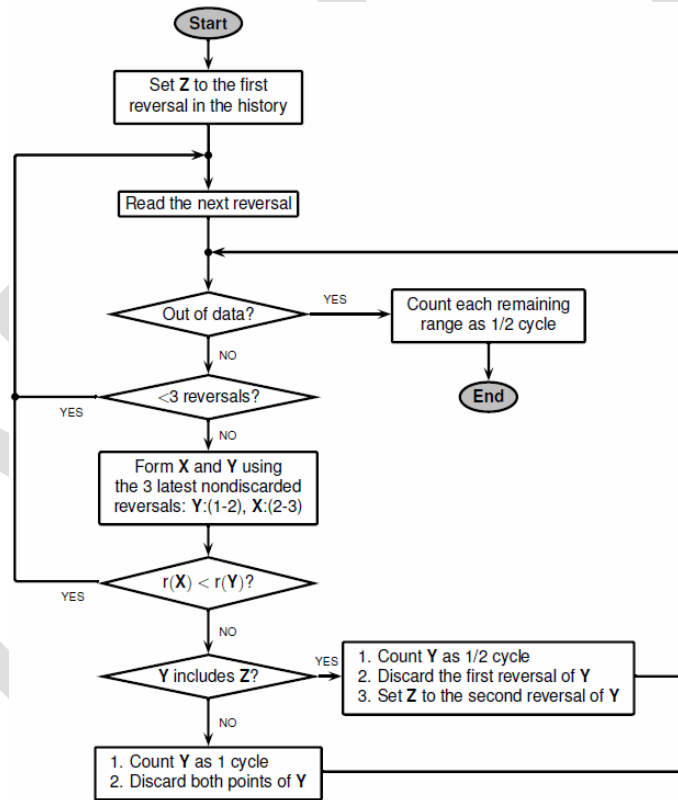


Figure 3. Diagram of Rainflow Counting.

Before running the rainflow algorithm, the data was run through a combination of Hysteresis and Peak & Valley Filtering. These filters were applied to remove “noise” peaks and valleys that were below 0.5 MPa (MathWorks).

3.4 Fatigue damage during the monitoring period and estimating the remaining lifetime.

Fatigue damage and remaining life are typically assessed according to S-N curves developed based on laboratory testing of small-scale steel specimens. “S” stands for stress and “N” stands for number of cycles to failure. Acknowledging the existence of multiple S-N curves and fatigue design documents that are potentially relevant to this work, DNV-C203 was selected as the S-N framework of choice (DNVGL-RP-C203, 2016). Most of the existing research on offshore wind turbines has utilized the DNV family of recommended practice documents. Figure 4 presents an example of “in air” S-N curves for different weld classes according to DNV-C203. In addition to S-N curves, Figure 5 contains annotations that describe the basic process of fatigue damage assessment. For each stress cycle bin, as defined by the rainflow cycle count, a ratio is formulated with the number of observed cycles and the number of cycles allowed in the S-N curve. These ratios are then added together for each stress cycle bin to find the total accumulated fatigue damage. If this accumulated damage is greater than 1 then the structure has exceeded the allowable fatigue capacity.

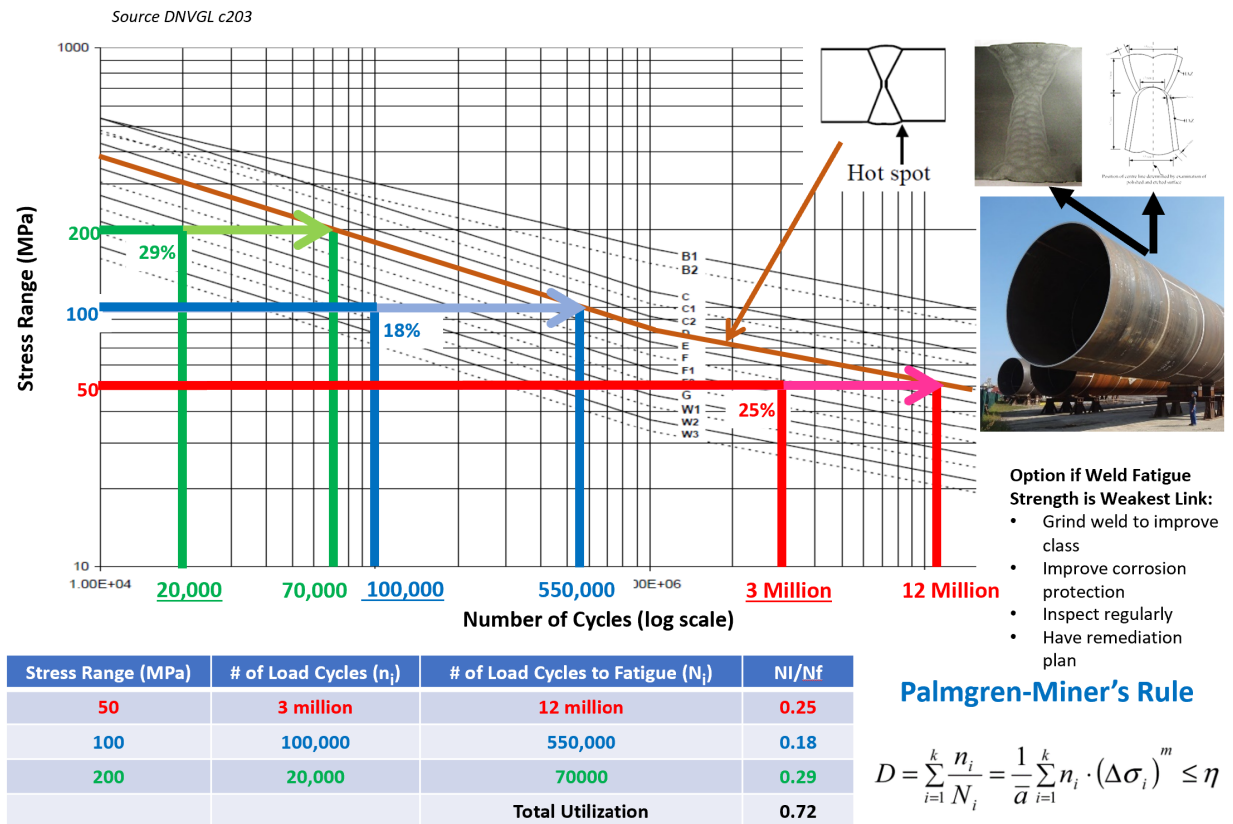


Figure 4. Example of S-N curve and simplified fatigue analysis.

One key feature of typical fatigue analysis with S-N curves is Palmgren-Miner's rule (DNVGL-RP-C203, 2016). Palmgren-Miner's rule assumes that fatigue damage accumulation is path independent, i.e., the sequence of loads does not matter. This simplifying assumption allows an engineer to add up the ratios without accounting for their placement in the time domain. The equation featured in Figure 4 is the following:

$$D = \sum_{i=1}^k \frac{n_i}{N_i} = \frac{1}{\bar{a}} * \sum_{i=1}^k n_i * (\Delta\sigma_i)^m \leq \eta \quad \text{Equation 5}$$

where the relevant variables are:

D : The total damage by fatigue from the time history.

n_i : The number of cycles observed in that stress bin from the rainflow counting.

k : The total number of stress bins.

N_i : The failure point on the S-N curve for the associated stress bin.

The value of N_i can be further broken down into the components of the S-N curve.

\bar{a} : The y-intercept of the S-N curve. Often given as $\log(\bar{a})$ since the linear regression done to make the curve is performed in log-space.

m : The slope of the S-N curve in log-space. It is either 3 or 5 depending on the curve and position on the curve.

η : The maximum allowable damage. This is typically 1. However, in cases with a design fatigue factor (DFF) this may be 0.5 or 0.33.

For this analysis, all S-N curves are based on the DNV C203 recommended practice document. B1 in air for base material was selected for the tower. C1 in air is selected for tower welds that are assumed to be ground. For the jacket, tubular and W3 welds are selected. In addition to selecting these two weld types, three different environmental conditions are analyzed: in-air, cathodic protection, and free corrosion curves. Table 1 provides an overview of all the constants that define the S-N curves seen in Equation 6.

$$\log(N) = \log(\bar{a}) - m * \log(\Delta\sigma) \quad \text{Equation 6}$$

Table 1. Constants for S-N curves.

| Weld Type | Environment | a1 | m1 | a2 | m2 |
|-----------|---------------------|--------|----|--------|-----|
| B1 | In-Air | 15.117 | 4 | 17.146 | 5 |
| C1 | In-Air | 12.499 | 3 | 16.081 | 5 |
| Tubular | In-Air | 12.48 | 3 | 16.13 | 5 |
| Tubular | Cathodic Protection | 12.18 | 3 | 16.13 | 5 |
| Tubular | Free Corrosion | 12.03 | 3 | N/A | N/A |
| W3 | In Air | 10.97 | 3 | 13.617 | 5 |
| W3 | Cathodic Protection | 10.57 | 3 | 13.617 | 5 |
| W3 | Free Corrosion | 10.493 | 3 | N/A | N/A |

Typical details of welding of the tubes (brace to leg) for the BIWF jacket are shown in Figure 5, provided in DNV C203. The curves that applied in this report to the BIWF jacket fatigue

assessment are the tubular joints with different environmental condition and the W3 curves for the partial penetration welds, as shown in section C of the typical weld. The assumption of the partial penetration is based on that the backup weld is not subject to inspection. This is a conservative assumption being made following the guidance in DNV C203 table A-10 for tubular members. For base material, a condition that is rarely relevant for fatigue, a tubular or T S-N curve can be used. If there is a partial penetration weld for a tubular member a W3 curve is recommended.

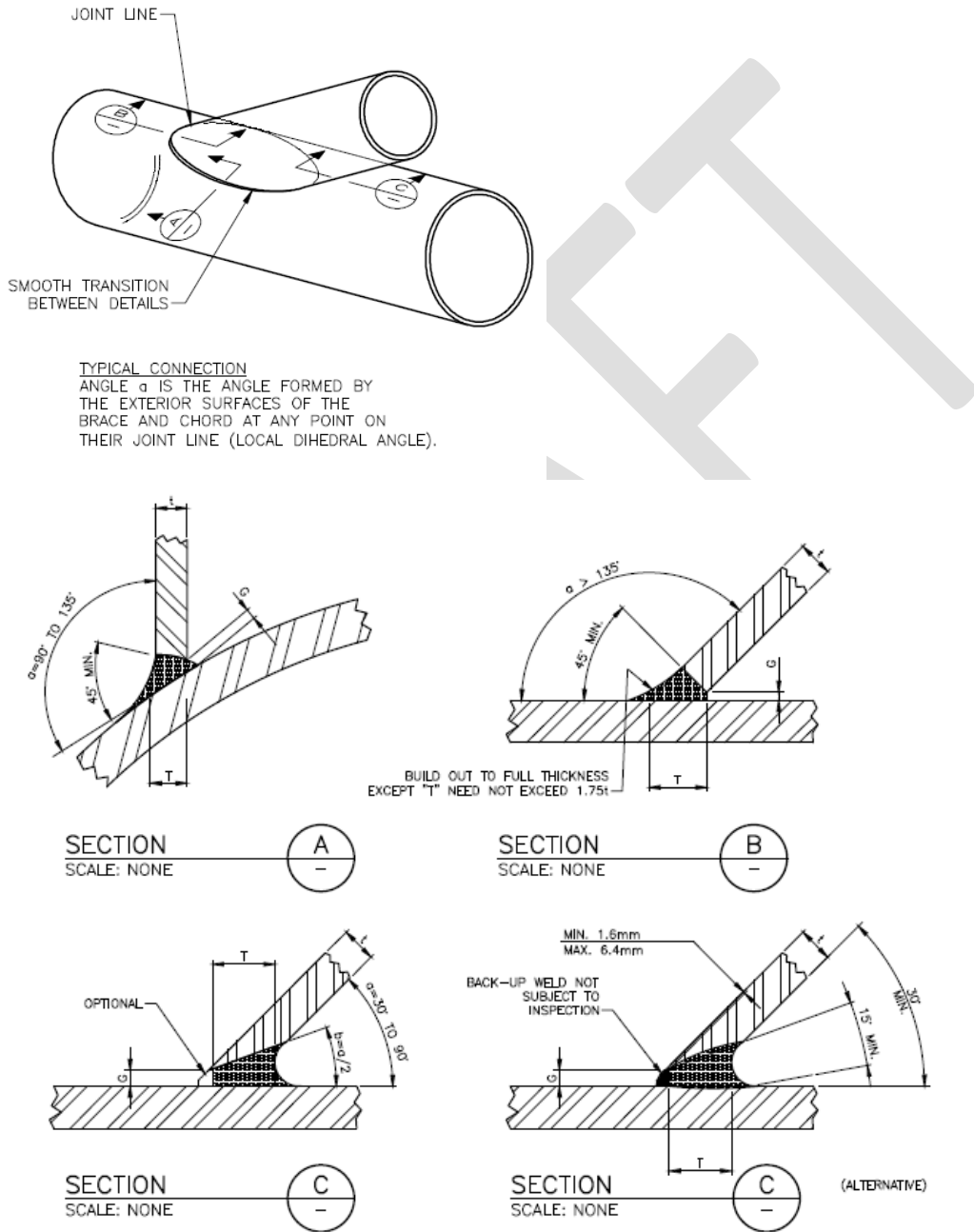


Figure 5. Typical welding details of the BIWF jacket foundation (figure credit: DNVGL-RP-C203, 2016).

The environmental conditions from Table 1 are described as follows.

- In-air curves represent material that is not exposed to any corrosive conditions. This includes parts of the structure far above the water such as the tower and material in the splash zone that is protected by an intact coating.
- Cathodic protection curves are used for material that is in the submerged zone of the structure and is protected with a cathodic protection system. Although corrosion information is not included in this report it is reasonable to assume that steel submerged in water was designed to be cathodically protected. According to DNV-RP-0416 section 4.4.2 “it is mandatory that external surfaces of the submerged zone shall have cathodic protection” (DNV, 2016).

Table 2. DFF Table 4-18 Taken from DNV-ST-0126

| <i>Location</i> | <i>Accessibility for inspection and repair of initial fatigue and coating damages ²⁾</i> | <i>S-N curve ⁵⁾</i> | <i>Minimum DFF⁶⁾</i> |
|--|---|---|---------------------------------|
| Atmospheric zone | No | In air for coated surfaces free corrosion for surfaces protected by corrosion allowance, only ⁴⁾ | 3 |
| | Yes | | 1 |
| Upper splash zone (above MWL) ¹⁾ | No | Combination of in air and free corrosion curves ^{3) 4)} | 3 |
| | Yes | | 2 |
| Lower splash zone (below MWL) ¹⁾ | No | In seawater for surfaces with cathodic protection Free corrosion for surfaces protected by corrosion allowance, only ⁴⁾ | 3 |
| | Yes | | 2 |
| Submerged zone | No | In seawater for surfaces with cathodic protection Free corrosion for surfaces protected by corrosion allowance, only ⁴⁾ | 3 |
| | Yes | | 2 |
| Scour zone | No | Free corrosion for surfaces protected by corrosion allowance, only ⁴⁾ | 3 |
| Below scour zone | No | In seawater | 3 |
| <p>Note:</p> <p>1) Splash zone definition according to DNVGL-RP-0416.</p> <p>2) If the designer considers the steel surface accessible for inspection and repair of initial fatigue damage and coating, this shall be documented through qualified procedures for these activities. See also [4.16] and Sec.9.</p> <p>3) The basic S-N curve for unprotected steel in the splash zone is the curve marked free corrosion. The basic S-N curve for coated steel is the curve marked in air. It is acceptable to carry out fatigue life calculations in the splash zone based on accumulated damage for steel considering the probable coating conditions throughout the design life – intact, damaged and repaired. The coating conditions shall refer to an inspection and repair plan as specified in Sec.9.</p> <p>4) When free corrosion S-N curves are applied in design, the full benefit of potential grinding of welds as outlined in [4.13.5] cannot be expected and therefore may not be taken into account. The effect of free corrosion on a ground weld may be accounted for by downgrading the S-N curve one class and applying the S-N curves for in seawater for free corrosion.</p> <p>5) Shear keys within grouted connections may be designed assuming S-N curves marked in air.</p> <p>6) According to the chosen DFF, an inspection program according to [9.3] will be required.</p> | | | |

Finally, when performing a fatigue design analysis there is an important design fatigue factor (DFF) applied as a safety factor to account for a variety of uncertainties including loading amplitudes, potential for defects/corrosion damage, and loading sequence. The design document DNV-ST-0126 Support Structures for Offshore Wind Turbines (2018) has a table that provides DFFs for foundation design (DNV, 2021). These DFFs depend on a variety of factors seen in Table 2.

4 The B2 Offshore Wind Turbine and its Monitoring System

4.1 Block Island Wind Farm

The Block Island Wind Farm (BIWF) became the first U.S. offshore wind farm in 2016 (Ørsted, 2016). It consists of five Haliade-X 6-MW OWTs operated by Ørsted. Turbines at the BIWF are labeled as B1-B6. Turbine B2 is instrumented with accelerometers and strain gauges (SGs) and has been continuously monitored.

4.2 Monitoring System of Strain Gauges

The monitoring system currently consists of 9 wired accelerometers, 4 wireless accelerometers, 8 strain gauges (SGs), and 1 inclinometer. The whole system, including sensors, cables, and data acquisition (DAQ) were designed and provided by the Norwegian Geotechnical Institute (NGI). The SGs were installed on October 24, 2021, and they have been providing measurements since then. They include 4 axial SGs and 4 circumferential SGs, which were paired one to one and installed on the inner side of the tower at about 0.5 m above the tower-to-deck connection bolts. The layout of accelerometers and SGs are shown in Figure 6. The axial strain gauges, that measure the strain along the tower's vertical axis, are labeled as SG135, SG225, SG315, and SG45 and located at 45°, 135°, 225°, and 315° from the platform North, respectively. SG45 and SG225 are located along the v-axis, and SG135 and 315 are located along the u-axis, as shown in Figure 1. The sampling frequency of the monitoring system is 50 Hz, and the data are stored in a series of 10 min long data sets. More detailed information about the instrumentation process and sensors can be found in Hines et al.(2023).

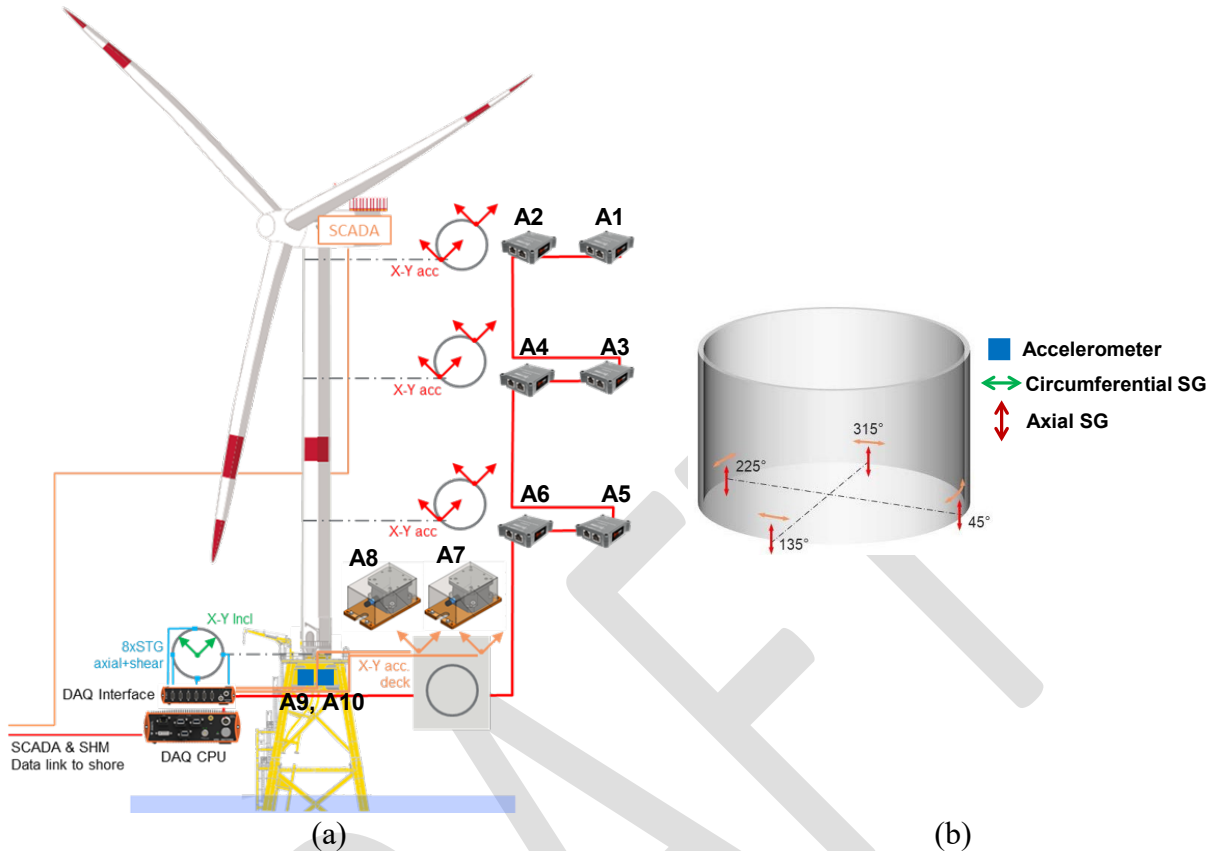


Figure 6. Elevation of the instrumentation plan (a) and (b) instrumented section of strain gauges (Hines et al., 2023).

4.3 Dataset Selection

Data measurements used for this study are for the months of November, December 2021, and January to October 2022. Each dataset consists of 10-minute SG time histories with a time step of 0.02 seconds. 144 datasets are available for every day and 4,032, 4,320, or 4,464 datasets every month with 28, 30, or 31 days, respectively. For the monitoring of a whole year, this results in 52,560 datasets, with some datasets missing due to inspection, etc. The total number of missing datasets, as shown in Table 3, is 4,735 which gives 47,825 total datasets being used in this report.

Data from the supervisory control and data acquisition (SCADA) system is also available for the BIWF-B2 turbine. The data gives relevant information about the turbine performance. SCADA data is missing from 6/19/2022 to 7/31/2022, and after 10/4/2022.

Table 3. The number of missing SG time history datasets used each month. Month 1 is November 2021 and month 12 is October 2022.

| Month | 1 | 2 | 3 | 4 | 5 | 6 | 7 | 8 | 9 | 10 | 11 | 12 | Total |
|------------|----|----|---|-----|-----|-------|-------|----|---|-----|----|-------|-------|
| # Datasets | 11 | 18 | 7 | 416 | 117 | 1,690 | 1,296 | 12 | 1 | 133 | 5 | 5,145 | 4,735 |

To match the SCADA time with the DAQ time, the clock should be adjusted. The DAQ clock had 17 minutes delay from the real time (SCADA time) in March 2023 while the delay was 5 minutes in June 2022. The clock offset for 12 months as follows. The clock offset is set to be zero for the

first 4 months: Nov. 2021 to Feb 2022, 10 minutes for the middle 4 months: Mar. to Jun 2022, and 20 minutes for the last 4 months: Jul to Oct 2022.

5 Experimental Results

In this section, we discuss the results from the tower and jacket fatigue analysis.

5.1 Fatigue Assessment of the BIWF-B2 Tower

To evaluate the tower fatigue, the data is filtered using the hysteresis method, and rainflow counting is used to evaluate the stress ranges and cycles. For example, the hysteresis filtering for one 10-min dataset is shown in Figure 7. A 3-D histogram of these results for is shown in Figure 8.

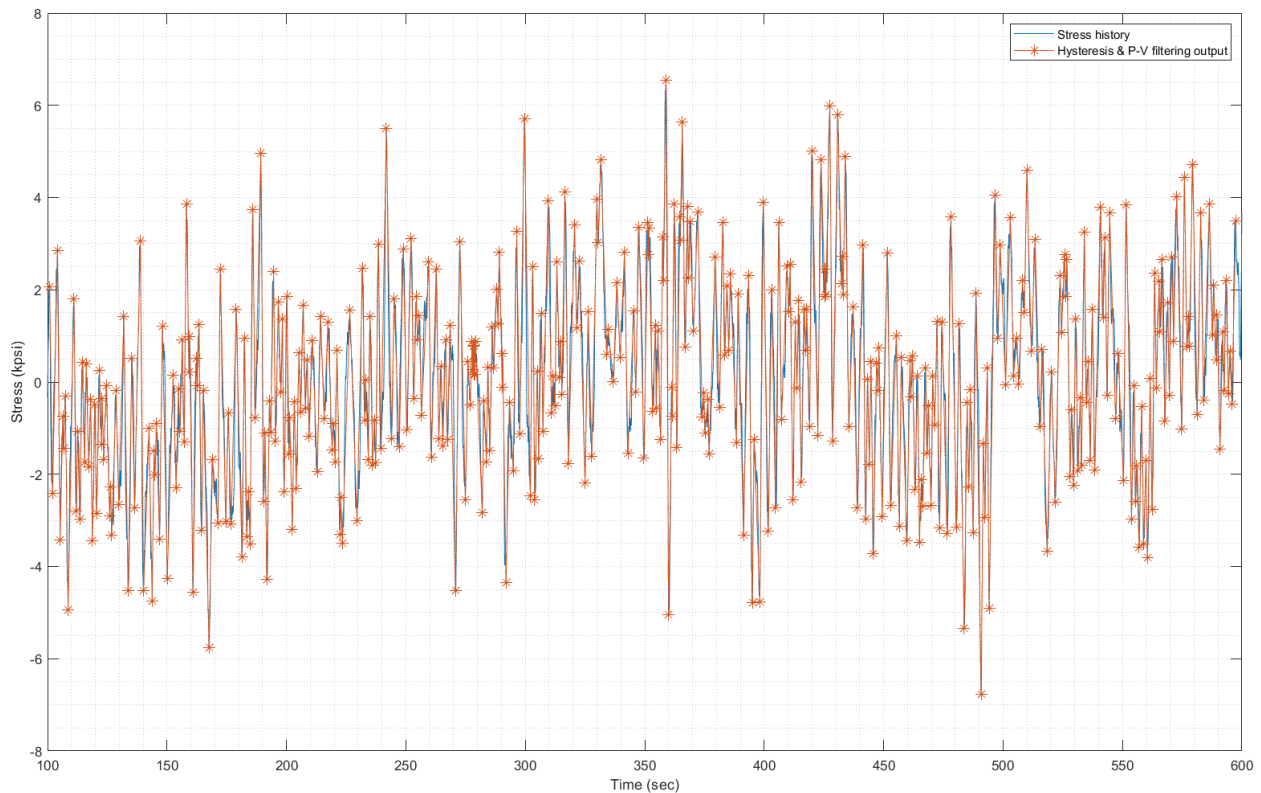


Figure 7. Hysteresis and Peak valley filtering for one 10-minute dataset in December 17, 2021 starting at 06:52 am.

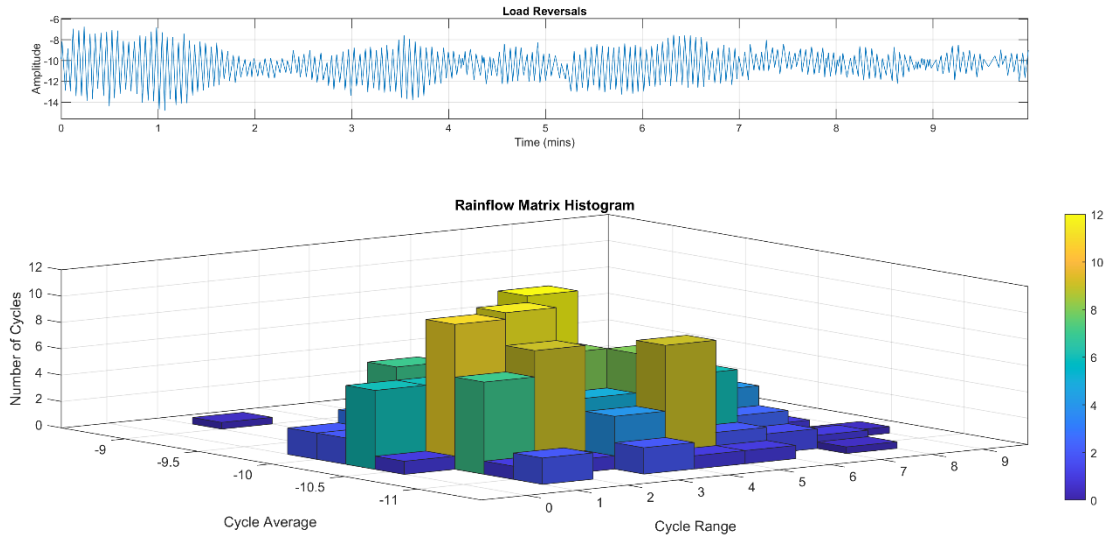


Figure 8. Rainflow counting for a 10-minute interval on December 17, 2021 starting at 06:52 am.

Table 4 and Table 5 show the raw and adjusted damage indices respectively for the tower at the strain gauges. The raw values in Table 4 come from directly adding damage indices from each 10-minute interval that was measured over the whole year. The adjusted values in Table 5 account for the fact that some months are missing. This is done by dividing the total damage indices for each month by the ratio of measured data/total time in month. Finally, Table 6 takes the reciprocal of the adjusted damage over one year to convert the adjusted damage in one year into an estimated lifespan in years.

The results in the tables also show the impact of the fatigue limit. According to DNV C203, a detailed fatigue analysis can be omitted if the largest local stress range is below the fatigue limit at 10^7 cycles. For the in-air curves the fatigue limit for the B-1 and C-1 curves are 106.97 MPa and 65.50 MPa respectively. As a result, fatigue damage is determined to be negligible for a B1 curve because all the stress cycles are below 100 MPa. However, for a C-1 curve most of the cycles are below 65.60 MPa but there are a few cycles above this limit, as seen in Figure 13. This means a fatigue analysis should still be done for the C-1 curve but the results indicate that fatigue is not driving design because the lifetimes are over 10,000 years at all the strain gauges.

Table 4. Raw Damage Indices Tower.

| | Raw Damage Indices (Over Year) | | | |
|---------------|---------------------------------------|--------------|--------------|--------------|
| Curve | SG45 | SG135 | SG225 | SG315 |
| B1 Air | Below FL | Below FL | Below FL | Below FL |
| C1 Air | 1.35E-05 | 1.22E-05 | 1.21E-05 | 1.55E-05 |

Table 5. Adjusted Damage Indices Tower.

| | Adjusted Damage Indices (Over Year) | | | |
|---------------|--|--------------|--------------|--------------|
| Curve | SG45 | SG135 | SG225 | SG315 |
| B1 Air | Below FL | Below FL | Below FL | Below FL |
| C1 Air | 1.56E-05 | 1.50E-05 | 1.39E-05 | 1.91E-05 |

Table 6. Estimated Lifespan Tower in Years.

| Curve | Estimated Lifetime Adjusted | | | |
|--------|-----------------------------|----------|----------|----------|
| | SG45 | SG135 | SG225 | SG315 |
| B1 Air | Below FL | Below FL | Below FL | Below FL |
| C1 Air | 6.43E+04 | 6.66E+04 | 7.20E+04 | 5.23E+04 |

Review of the results in the preceding tables yields the following observations.

- The adjusted damages are slightly higher than the damages identified by our raw data. This is due to the missing data from each month seen in Figure 9.
- There is a clear sensitivity to the plate detail used in the fatigue analysis. Between a B1 curve representing a theoretical base material and a C1 curve representing a high quality, ground, circumferential weld there is an order of magnitude difference E-6 vs E-5.
- For the estimated 25-year lifetime we see there is not a significant amount of fatigue damage observed. When estimating the remaining life in Table 5 the lowest value is 52,000 years.

Based on the observed data it is unlikely that there would be any major fatigue concerns for the tower base material at the location of the strain gauges, suggesting that fatigue concerns be directed toward areas of stress concentration such as the flange detail or to the bolts connecting the tower to the transition piece, which are known to experience tension losses over their lifetime.

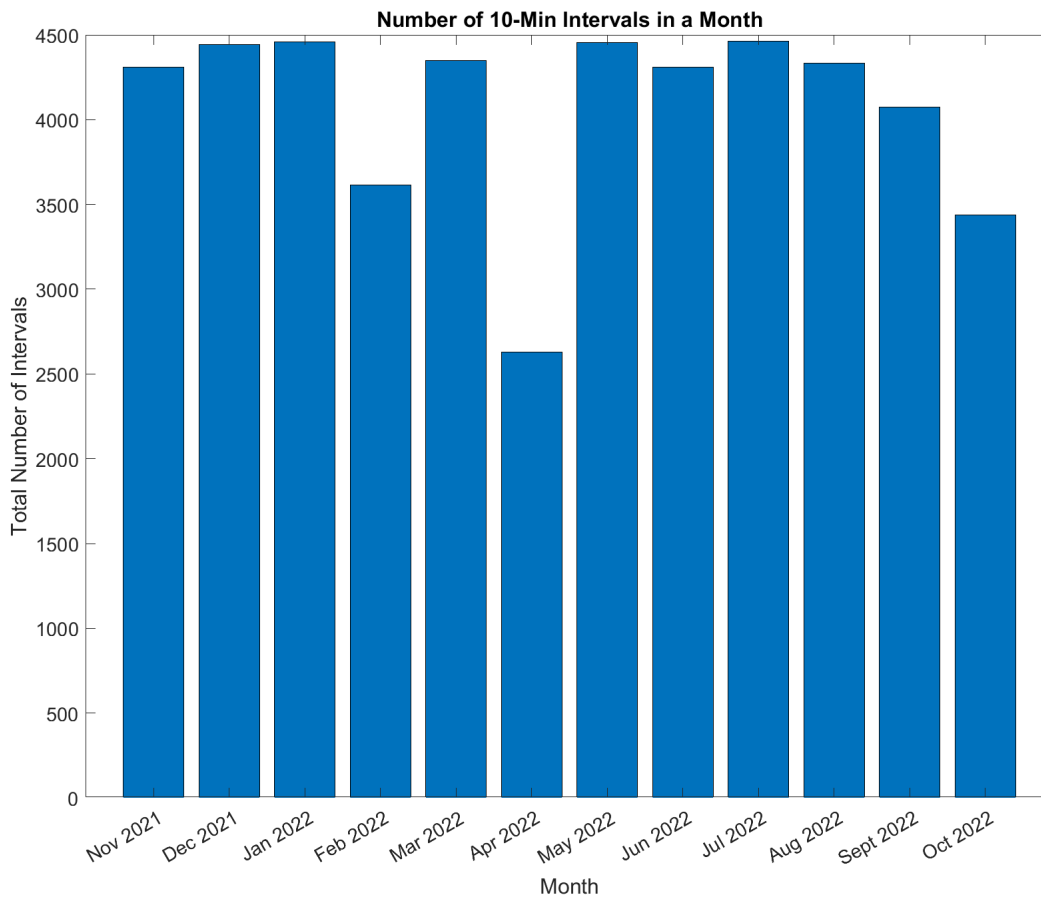


Figure 9. Number of 10-Minute Intervals Observed in Each Month.

5.1.1 Sources of Fatigue Damage in Tower

The previous analysis indicates that fatigue is not likely to be a driver of tower design at the base of the tower where the strain gauges are placed. Nevertheless, a relative comparison of the data can still provide an interesting perspective about what events, stress cycles, and conditions drive most of the observed fatigue damage. Figure 10 shows a breakdown of the raw damage observed during each month.

When looking at Figure 10 it is important to remember that April, the month with the highest observed damage, is also the month with the lowest number of observed stress cycles. The damage occurring in the month of April is almost twice as high as the next highest month.

Figure 11 is a cumulative plot showing how the damage accumulates across the month of April and it shows that in the month of April there are sections with very steep slopes. This would seem to indicate that the damage accumulation in April comes from discrete events occurring rather than a higher amount of damage occurring over the typical operational conditions of the turbine. Figure 12 is the same cumulative damage plot for June that shows a lack of the large jumps seen in April.

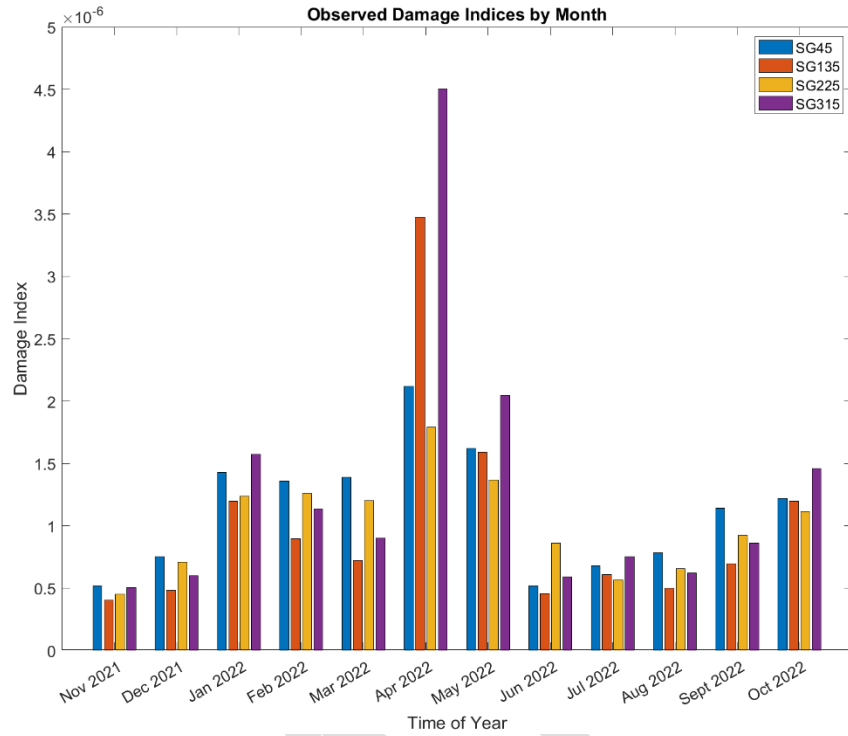


Figure 10. Raw Data of Damage Breakdown by Month.

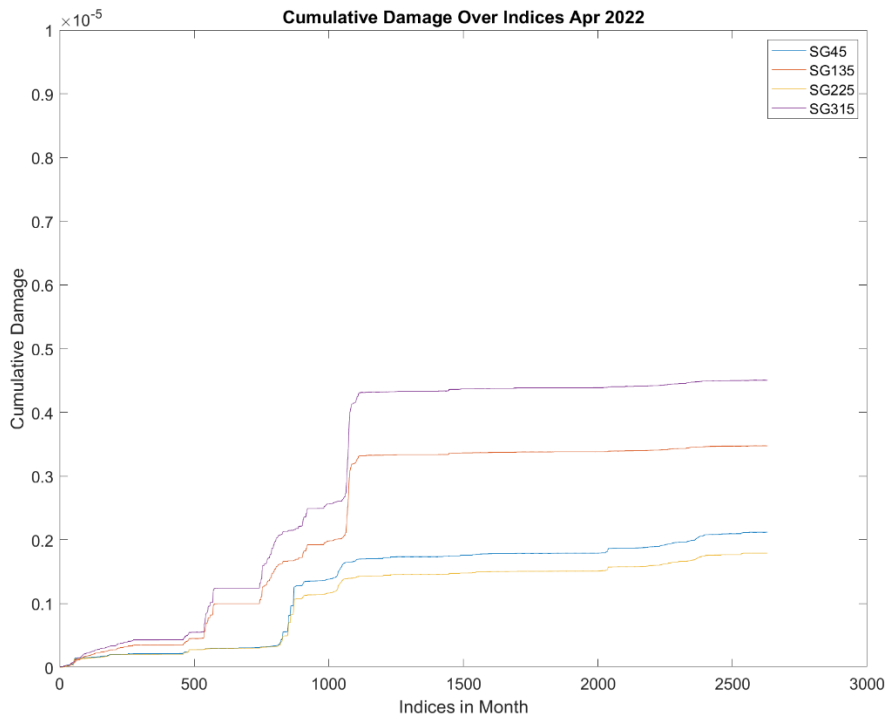


Figure 11. Damage Accumulation in the Month of April.

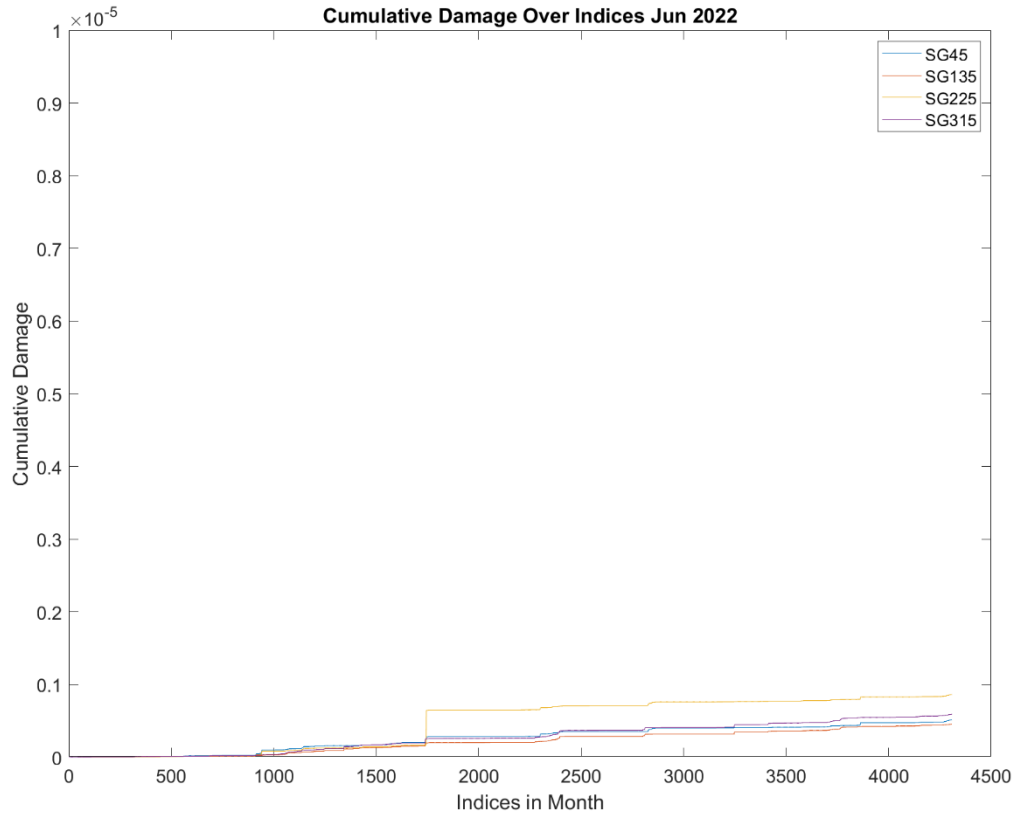


Figure 12. Damage Accumulation in the Month of June.

After observing that damage does seem to jump during events with some relation to time instead of keeping a constant slope the next step was to analyze how damage was associated with the stress bins. Figure 13 plots the damage from each 0.5 MPa stress bin across the entire year. Here there is a clear mass from 10-30 MPa where most of the damage is occurring. Then above 30 MPa there is still damage occurring, but the trend is less clear, and it does not look like a clean curve. To get a better sense of when these large stress cycles are occurring the same kind of figure is shown for just the month of April (Figure 14) and the month of June (Figure 15). Comparing Figure 14 and Figure 15, the month of April has more damage occurring from the high stress cycles than June.

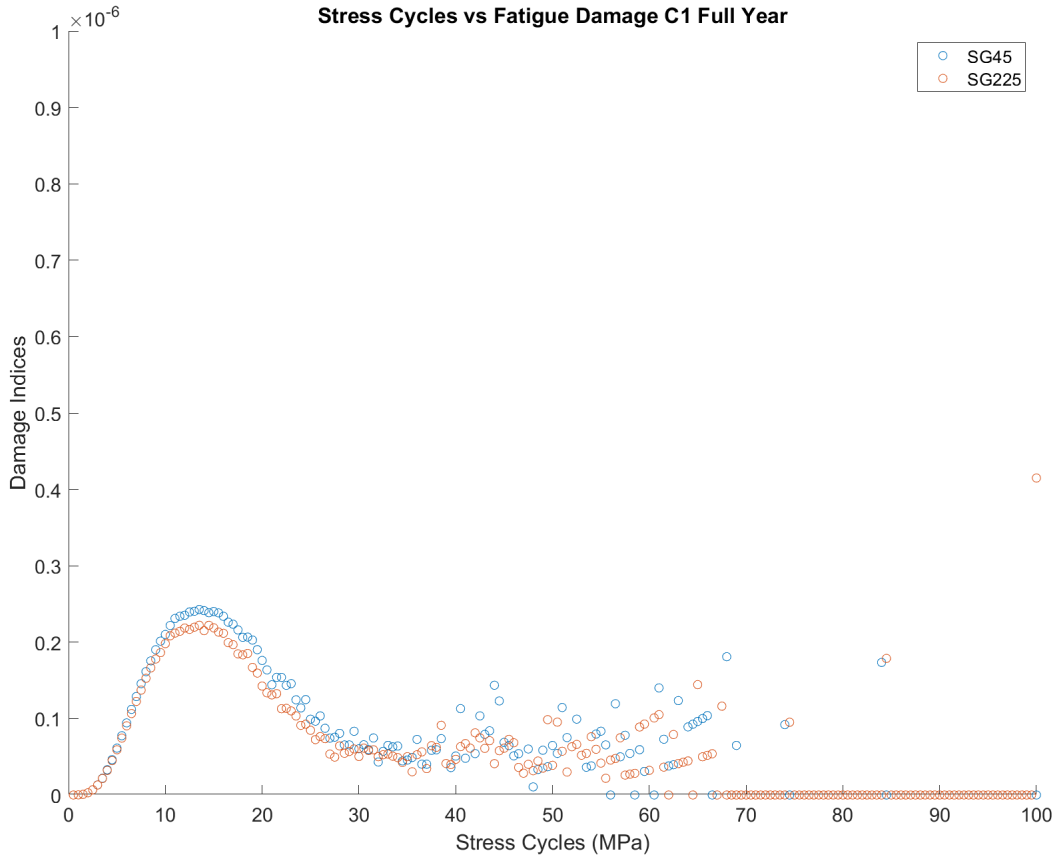


Figure 13. Damage by Stress Range Full Year.

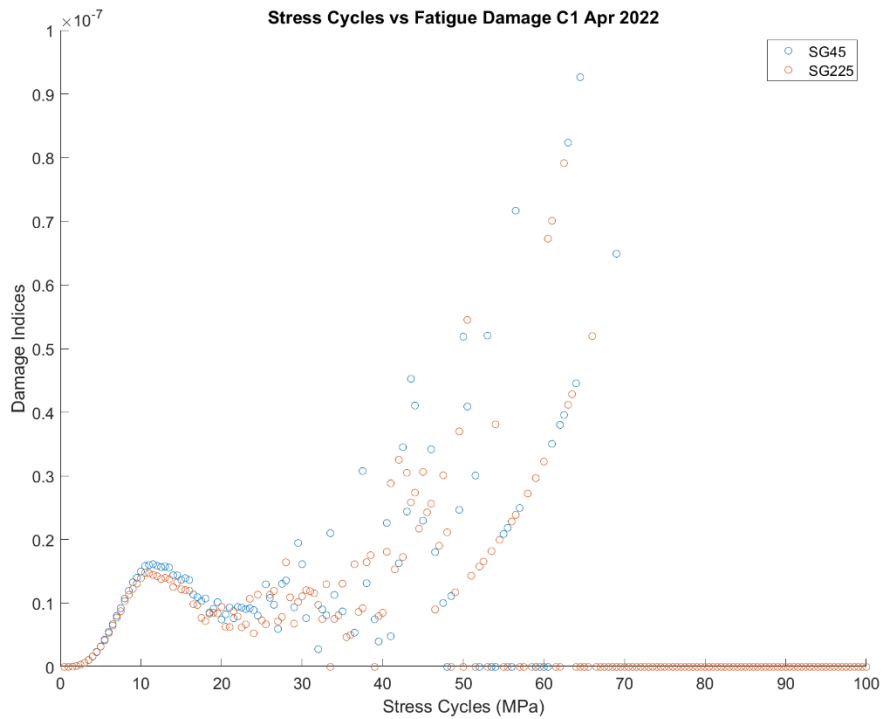


Figure 14. Damage by Stress Cycle April.

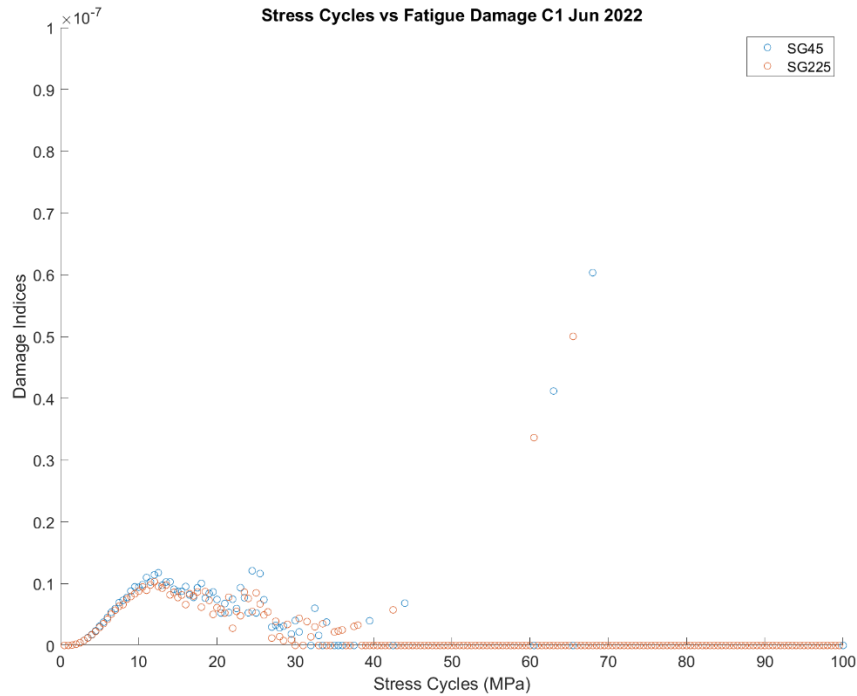


Figure 15. Damage by Stress Cycle June.

5.1.2 Time Series Investigation

Based on the analysis of the months and the stress cycles there appears to be at least two categories of operation. First there are 10-minute intervals that do not account for a significant amount of the damage measured in the tower. Second there are intervals that provide more damage. This can be seen in Figure 11 and Figure 12 for cumulative damage. The comparison between Figure 14 and Figure 15 also show that there does appear to be something unique about April when looking at the relative damage from high stress cycles above 30 MPa.

Based on this evidence additional scrutiny was placed on the month of April. Looking at the time series for the 10-minute intervals with the highest Damage indices there are some interesting patterns. Figure 16 shows a time series for the file name 2022_09_12_093019. This is a representative example. Looking at the time series there is a clear “event” that occurs and causes a large half cycle during these time series. After reviewing the 10-minute average SCADA data it appears that this “event” occurs when the blades pitch changes from pitch angle of -1.5° to fully feathered blades with pitch angle of 90° . It is difficult to identify the precise moment when this event occurs since the SCADA data is only in 10-minute intervals, but the response of the structure looks like a classic free vibration with damping. During the event, the FA moment also changes a lot from $+30$ MN m to about -20 MN m.

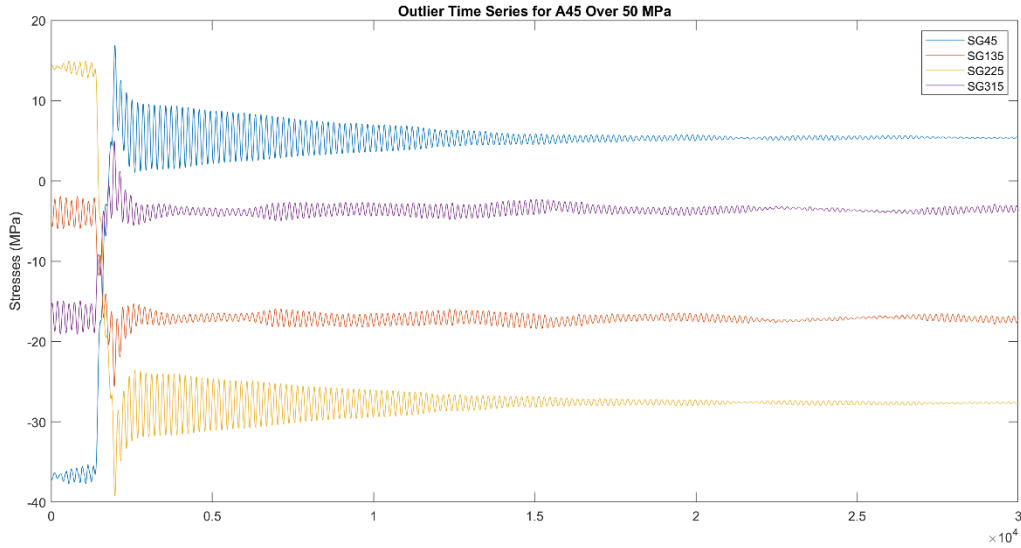


Figure 16. Stress time history during 10-min window starting on Sep. 12, 2022, at 09:30 am.

5.2 Fatigue Assessment of the BIWF-B2 Jacket

In this section, we show the results for the jacket fatigue analysis. We picked three critical joints on the jacket legs and braces to estimate the damage during the 1-year monitoring of the turbine. We then estimate the lifetime of the joints by assuming that the damage in the upcoming years would be the same as the 1-year damage results.

5.2.1 Stress estimation at jacket joints

For this report, a 1 MN load is applied at the RNA level at 4 different angles: 0° , 15° , 30° , and 45° as shown in Figure 17, to estimate the stresses in the jacket members. The Von Mises stress (S_{11}) in a member section is obtained in 8 stations around the perimeter of the section, as shown in Figure 17.c. The stress hotspot to do fatigue analysis should be chosen at welds between the braces and the tubular joint. We chose Station 3 for the leg joints and the maximum between 8 stations for the braces. The result for each angle is shown in Table 7.

The maximum S_{11} between all the angles is chosen as the stress for the leg/brace joints, as shown in Figure 18. The studied joints are on one leg of the jacket and the braces in seawater and one leg in the splash zone. The stresses are then used linearly estimating the stress by scaling the thrust force from a 1 MN to any other Thrust force over time.

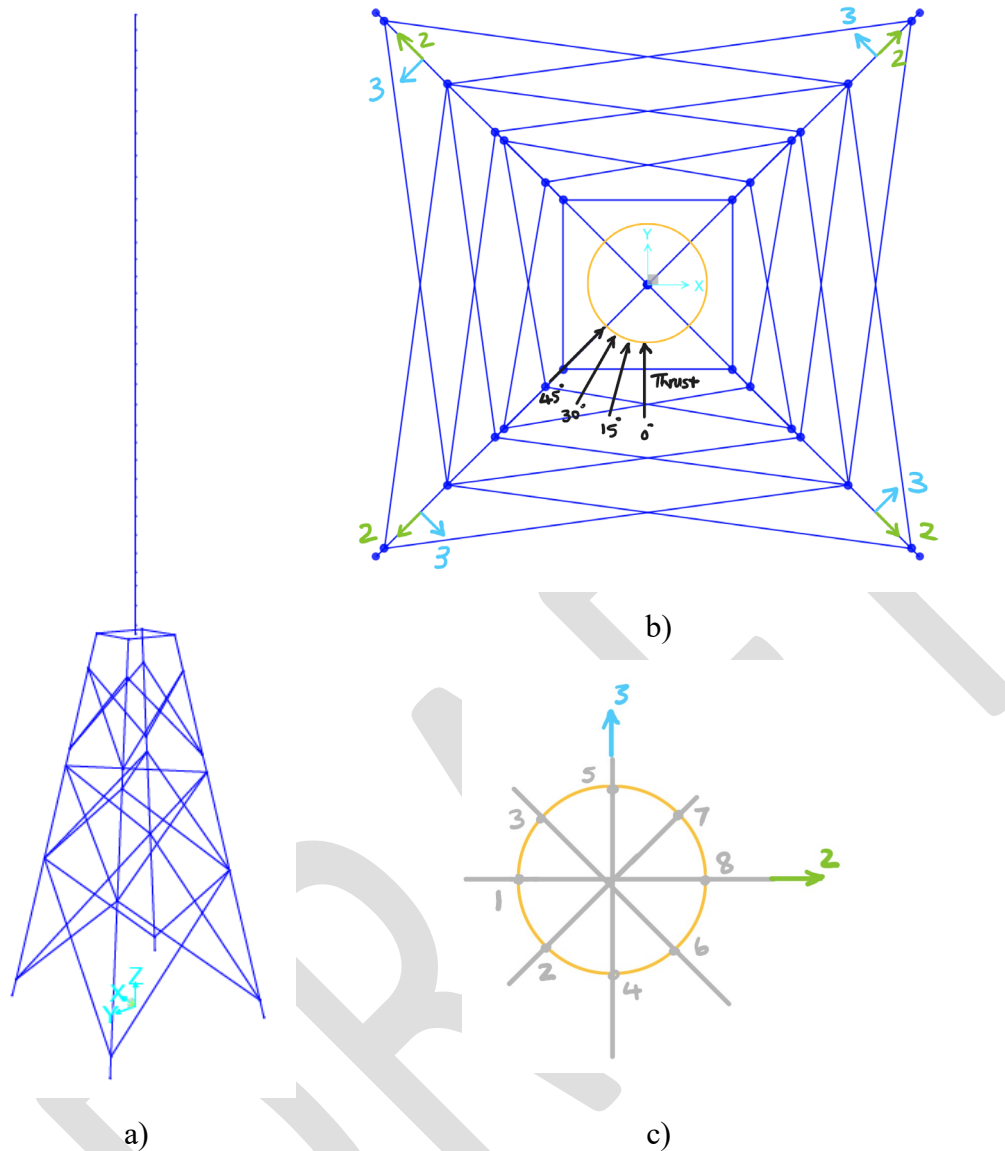


Figure 17. a) 3D view and b) Top view of the BIWF-B2 turbine in SAP2000 tool (not to scale), and c) one beam element section with 8 stations; the local axes 2 & 3 in c) are also shown in the global coordinates in b). * All local coordinates on the foundation elements are provided in Appendix A.

Table 7. Stresses at several sections in legs and braces of the BIWF jacket (MPa/1 MN).

| Angle \ Joint | 1 | 2 | 3 | 4 | 5 | 6 |
|---------------|-------|-------|------|-------|------|------|
| 0° | -55.5 | ±8.6 | 45.1 | ±9.5 | 52.4 | 58.3 |
| 15° | -65.0 | ±9.8 | 53 | ±16.8 | 57.0 | 64.4 |
| 30° | -66.9 | ±11.4 | 59.6 | ±15.3 | 83.9 | 66 |
| 45° | -70.3 | ±11.7 | 61.7 | ±12.9 | 84.1 | 63.2 |

The chosen jacket joints for the fatigue analysis and their stress ratios to 1 MN thrust force are shown in Figure 18. Three critical joints were picked based on their stress values. The chosen

joints are Joint #1: leg joint and Joint #2: brace joint in seawater with cathodic protection and Joint #5: leg joint in splash zone without cathodic protection.

| Joint | Angle (°) | FA mode S11 max (MPa/1MN) | In Air/ Water | Cathodic Protection |
|-------|-----------|---------------------------|---------------|---------------------|
| 1 | 45 | -70.3 | W | Yes |
| 2 | 45 | 16.8 | W | Yes |
| 3 | 45 | 61.7 | W | Yes |
| 4 | 15 | 11.7 | W | Yes |
| 5 | 45 | 84.1 | Splash zone | No |
| 6 | 30 | 66.0 | Splash zone | No |

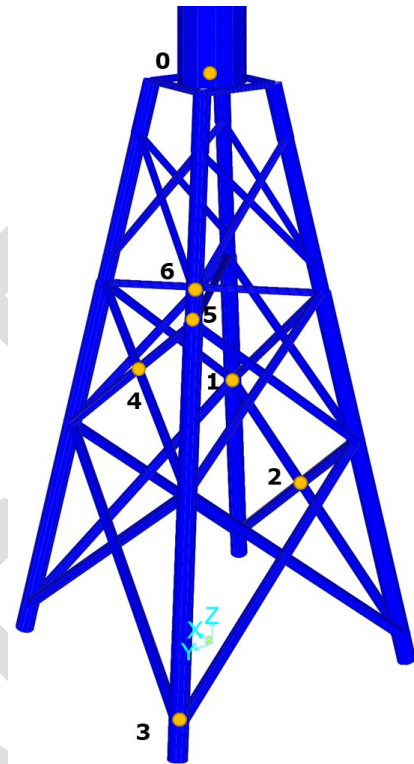
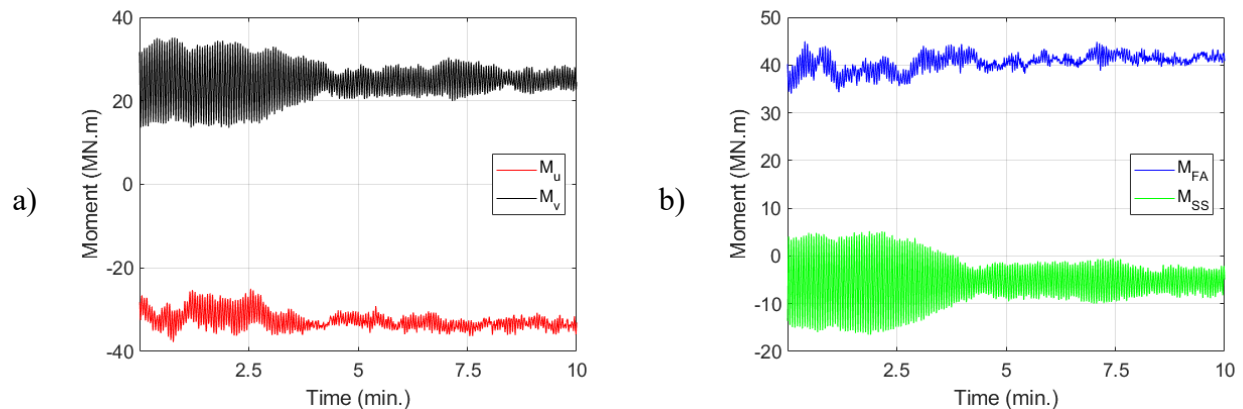


Figure 18. jacket nodes stresses obtained from the FE model due to 1 MN thrust force at the RNA level.

The estimation of stress on the selected jacket Joints (#1, #2, and #5) for one 10-minute dataset in September 2022 is shown in Figure 19. d. The dataset is selected based on the turbine’s operational condition. It is one of the datasets that has approximately maximum thrust. The estimation was based on the product of the stress values in Figure 18 to the thrust in Figure 19. C. The calculation of thrust is discussed in Section 3.2.



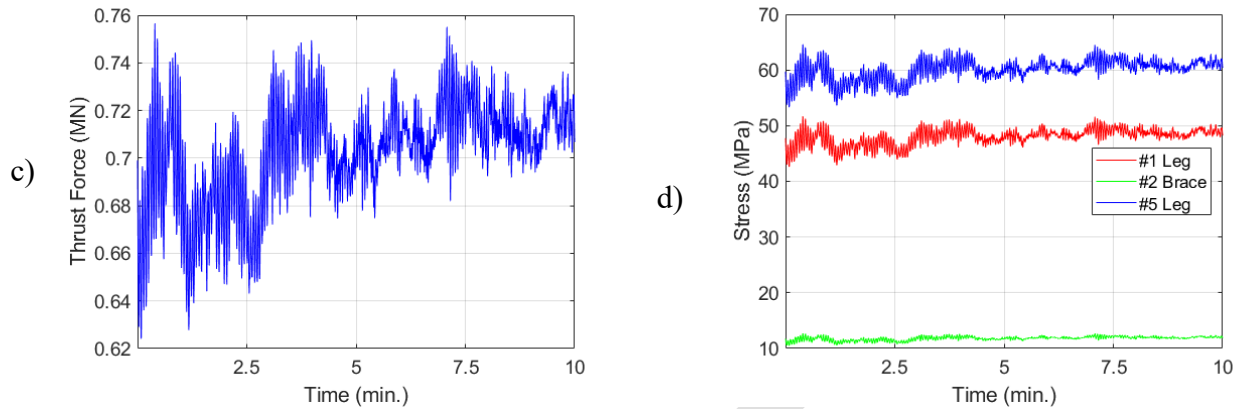


Figure 19. a) moments in (u, v) coordinates, b) moments in FA, SS directions, c) thrust force, and d) jacket Joints stresses for a 10-min interval of SG data starting at 26-Sep-2022 16:53 pm.

5.2.2 Damage and Fatigue life estimation

The stress data goes through the same hysteresis filtering and rainflow counting process used for tower fatigue. The cumulative results for damage during May 2022, which is one of the months with higher damage, is shown in Figure 20. Joint #5 – leg in the splash zone has more damage than Joint #3 – leg in seawater. The brace doesn't have significant fatigue damage compared to the leg joints. The damages for Joints #1 and #2 are calculated using W3 and tubular joint curves in seawater with cathodic protection. The damage for Joint #5 was calculated using W3 curve in air assuming the coating in the splash zone remains intact for the full 25-year lifespan. The curves are chosen based on the details of welding in the jacket drawings, discussed in Section 3.4. The cumulative damages for other months are provided in Appendix B.

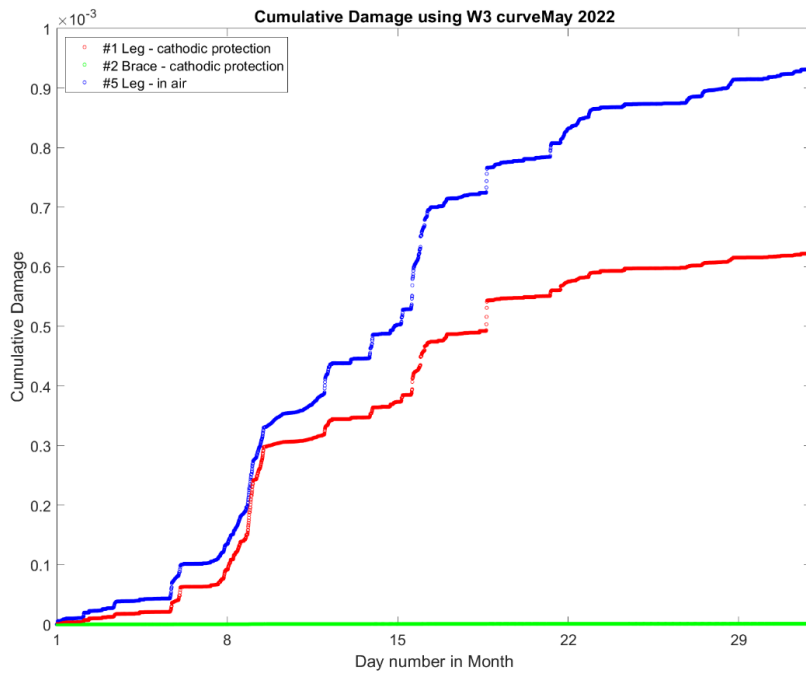


Figure 20. Cumulative damage in jacket nodes during May 2022.

The cumulative damage estimate for a 25-year lifetime of the B2 turbine jacket is shown in Figure 21. The results show that the jacket legs will survive for the lifetime of the turbine with damage less than 25%. Considering DFF of 3 for the jacket leg in seawater, and 2 for the leg in the splash zone, the joint leg in seawater still would not fail after 25 years. If an in-air S-N curve is used for the whole lifetime of the structure the total damage at the splash zone joint #5 is only around 0.2, well below the failure point of 1.0 even with a DFF of 2 applied.

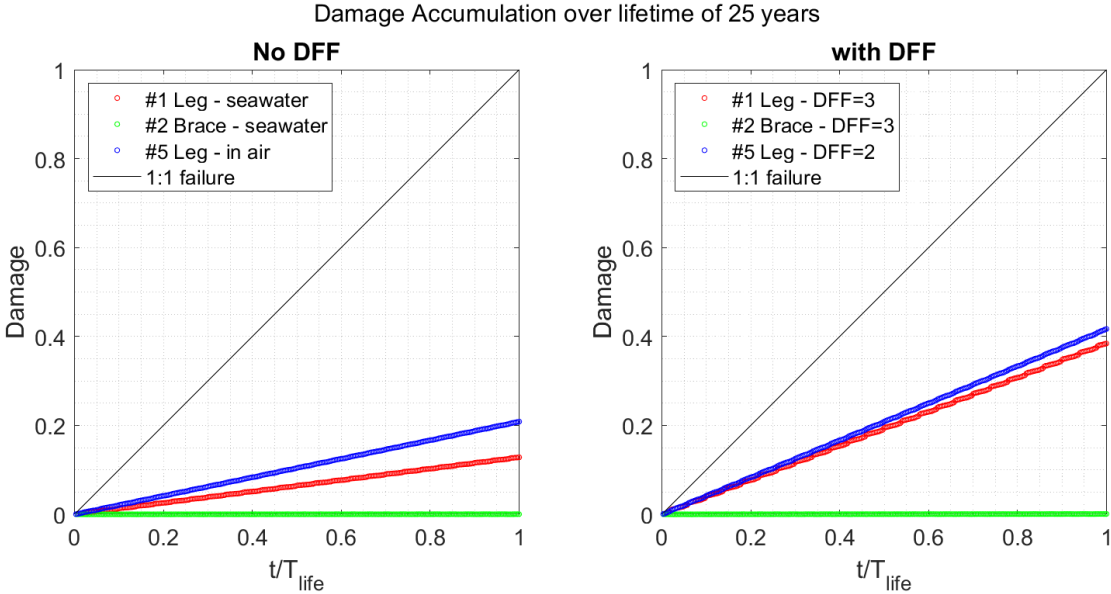


Figure 21. Damage vs. time ratio to the lifetime of 25 years using extrapolating 1-y monitoring results.

The cumulative damage over 1-year monitoring for the jacket joints using different curves are shown in Table 8. Comparing the results obtained from the tubular joints (first three rows) and the W3 curves (the last three rows of the table) shows that fatigue damage is larger using the W3 curve than the tubular joint curve.

Table 8. Damage Indices for the jacket joints during 1-year monitoring from Nov 2021 to Oct 2022 (no DFF used).

| Damage During one year of monitoring | | | |
|--|----------|----------|----------|
| Joint | 1 | 2 | 5 |
| Tubular joint with cathodic protection | 2.47E-05 | 2.86E-08 | 7.38E-05 |
| Tubular joint in seawater (no protection) | 7.37E-04 | 1.45E-05 | 1.41E-03 |
| Tubular joint in air | 2.44E-05 | 2.86E-08 | 6.80E-05 |
| W3 with cathodic protection | 5.12E-03 | 9.33E-06 | 1.27E-02 |
| W3 free corrosion | 2.54E-02 | 4.99E-04 | 4.87E-02 |
| W3 in air | 3.37E-03 | 8.88E-06 | 8.03E-03 |

The lifetime estimation of jacket joints is shown in Table 9. Table 10 provides a summary of the fatigue assessments from this work compared to the design estimates, reported in the BIWF sub-structure and foundation design documents (Keystone, 2015). The lifetime estimation for Joint #1 – leg joint is 195 years and with a DFF of 3, it becomes 65 years. The design fatigue life for Joint #1 reported is 26 years according to the design report which is less than the monitoring results. The method we use to assess the fatigue life of jacket using 1-year monitoring (e.g., 65 years for

joint#1) is conservative, so the estimated remaining lifetime could be larger in reality when different assumptions such as considering multi-directionality are made.

Table 9. Lifetime estimation of jacket joints based on the results from 1-year monitoring from Nov 2021 to Oct 2022 (no DFF used) .

| Lifetime Estimation (years) | | | |
|-----------------------------|-----|-------|-----|
| Joint | 1 | 2 | 5 |
| W3 with cathodic protection | 195 | * | 79 |
| W3 free corrosion | 39 | 2,003 | 21 |
| W3 in air | 297 | * | 124 |

* Extremely low fatigue demand

The lifetime estimation for Joint #5 – leg joint is 124 years for coated joints. However, considering a DFF of 2 changes it to 62 years which is greater than the fatigue life of 50 years reported in the BIWF sub-structure and foundation design documents (Keystone, 2015). Finally, the lifetime estimation for Joint #2 -brace joint yields an extremely low fatigue demand. Altogether, all three joints have estimated service life greater than the specified 20 year design life for the B2 turbine.

Table 10. Service life comparison between the extrapolation of 1-y monitoring and design values using DFF. DFF=2 and 3 are used for the environment of seawater and splash zone, respectively.

| Lifetime Estimation (years) | | | | |
|-----------------------------|-----------------------------|-----|-------------------|--------|
| Joint | Environment | DFF | 1-year Monitoring | Design |
| 1 | W3 with cathodic protection | 3 | 65 | 26 |
| 2 | W3 with cathodic protection | 3 | * | 76 |
| 5 | W3 in air | 2 | 62 | 50 |

* Extremely low fatigue demand

5.2.3 Effects of environmental/operational conditions on damage

In this section, the effects of environmental/operational conditions such as wind speed, rotor speed and pitch angle of the blades on the damage index and cumulative damage of the jacket at joint #5 are investigated.

As shown in Figure 22, higher damage indices occur around two different wind speeds:

1. Wind speed around 5 m/s where turbine starts to operate (startup condition); and
2. Wind speed around 10-11 m/s which turbine produces the maximum power, and the Thrust is maximum.

The highest damage index in Figure 22 is $4.42e-5$ and it is associated with consistent pitch angle of -1.5° . The SCADA data for that dataset and its nearest neighbors are shown in Table 11. The stress history and rainflow count for this dataset are shown in Figure 23. The rainflow plot shows there are a significant number of stress cycles between 5-45 MPa. Each stress range has a great contribution to the damage calculation.

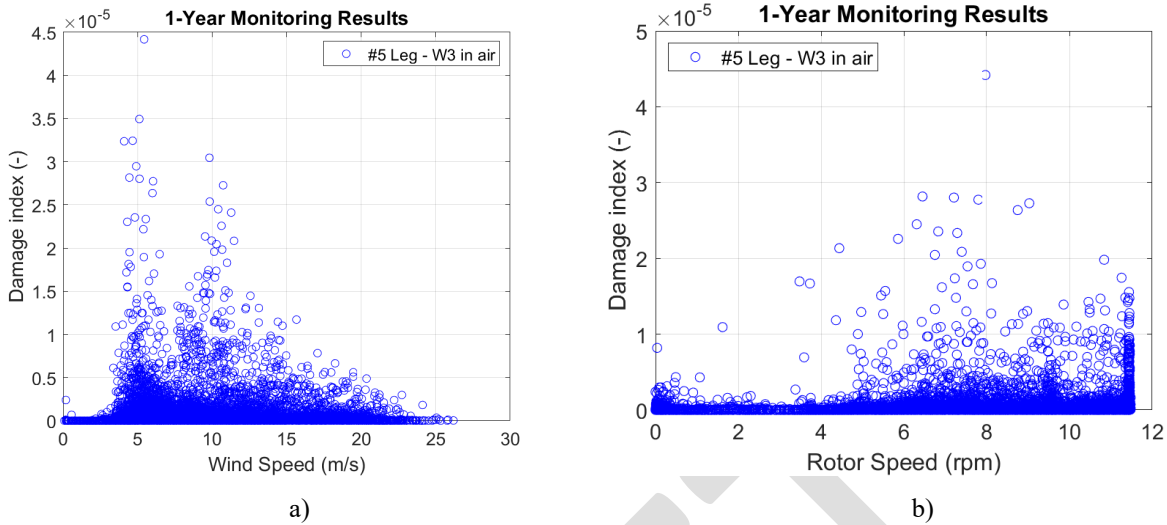


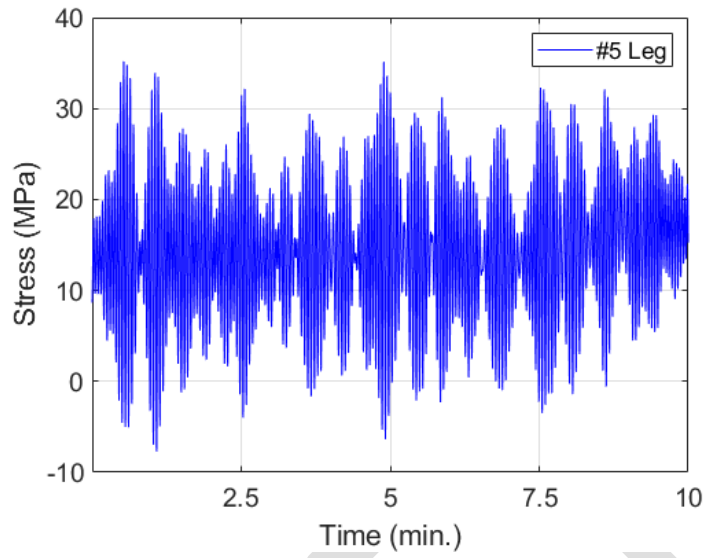
Figure 22. Effects of a) wind speed and b) rotor speed on the damage indices of the Jacket joint #5.

Table 11. SCADA for the highest damage index during 1-year monitoring caused by the dataset 2022_03_24_211556 (24-Mar-2022 at 21:10 pm), one SCADA before and after that dataset.

| SCADA TimeStamp | Wind Speed (m/s) | Power (MW) | Rotor Speed (rpm) | Yaw Angle (°) | Pitch Angle (°) | Damage Index (-) |
|-----------------------|------------------|------------|-------------------|---------------|-----------------|------------------|
| 24-Mar-2022 21:00:00' | 6.39 | 1676.06 | 8.88 | 33.6 | -1.5 | 1.27e-05 |
| 24-Mar-2022 21:10:00' | 5.44 | 1179.98 | 7.97 | 38.8 | -1.5 | 4.42e-05 |
| 24-Mar-2022 21:20:00' | 4.84 | 729.58 | 6.94 | 47.14 | -1.5 | 4.32e-06 |

High damage indices also occur as rotor speeds increase between 5 to 11.5 rpm. This represents the start-up phase of the turbine as the blades spin faster to increase power production. Another key variable that impacts the damage index is the pitch angle of blades. As shown in Figure 24, the high damage values are also associated with the change in the pitch angle of blades from 0 to 90° while the turbine is operating. One theory for why high damage indices is associated with a change in blade pitch is that when the blades suddenly feather and reduce the thrust load the tower moves in the fore direction because of the eccentric position of the nacelle mass. Without any thrust load from the feathered blades the tower and nacelle then oscillate freely. Figure 16 is a time series from the tower that may represent this kind of event. However, further interpretation of the relationship between these variables and the observed fatigue damage is limited by the resolution of available SCADA data. While the 10-minute averages are very helpful and provide useful information, higher resolution information on important variables such as blade pitch would allow for additional investigation.

a)



b)

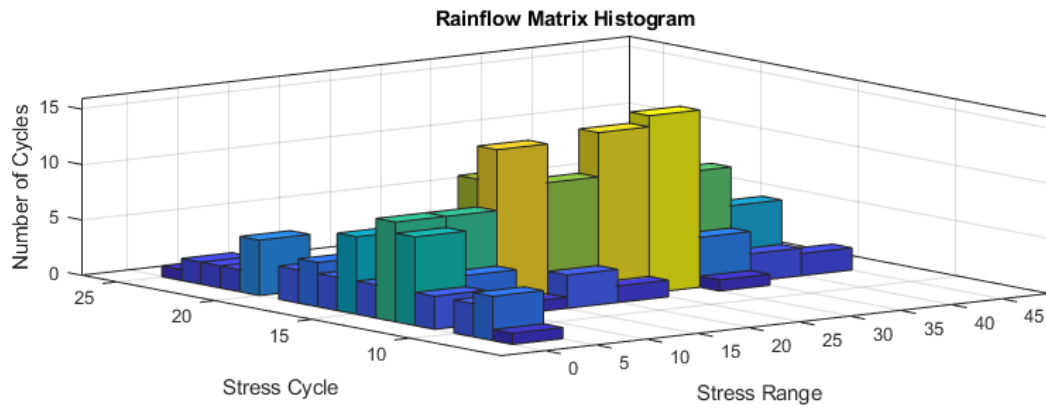


Figure 23. a) stress and b) rainflow counts of the stress of the Jacket leg joint #5 during one dataset on Mar. 24, 2022: 2022_03_24_210556, that has the largest damage index ($4.42e-05$) during 1-year monitoring.

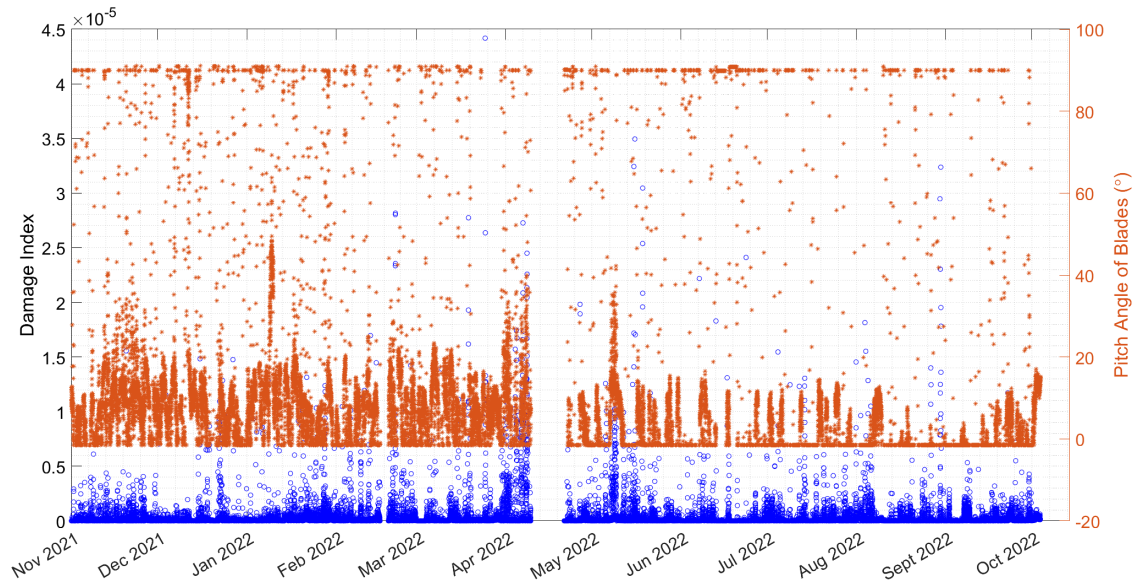


Figure 24. Damage index for the Jacket joint #5 vs. pitch angle of blades during 1-year of monitoring from Nov. 2021 to October 2022.

The plots for April and May 2022, both of which have large damage indices, are shown in Figure 25 and Figure 26. Although there are many factors affecting the damage index (e.g., wind speed and rotor speed), the pitch angle appears to play an important role. The peaks of damage index and pitch angle occur at approximately the same time. Moreover, the change in pitch angle of blades, where the blades change from facing the wind to fully feathered, creates a jump in the cumulative damage plot, seen in Figure 27 and Figure 28.

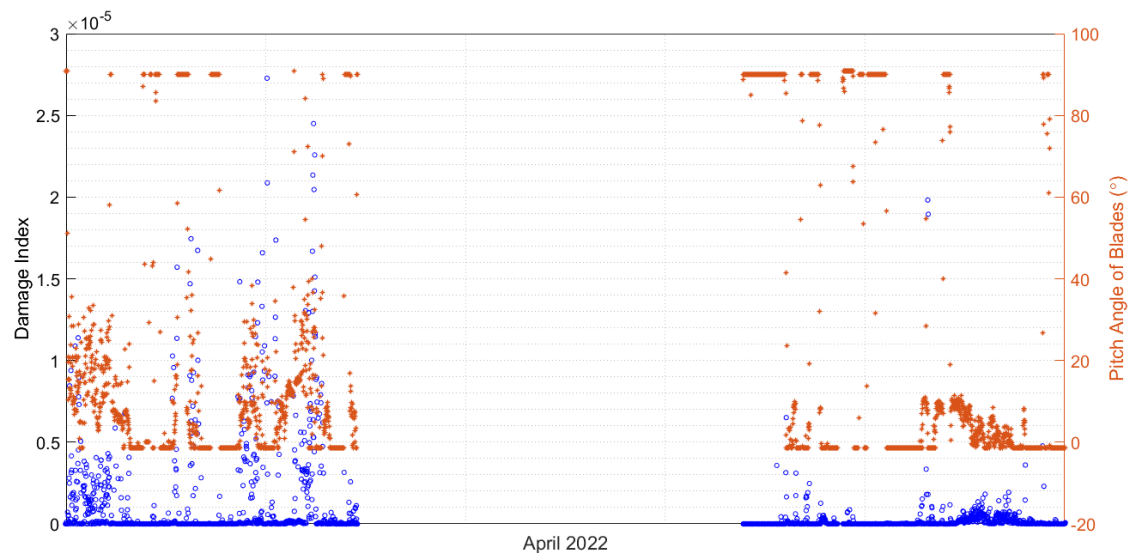


Figure 25. Damage index for the Jacket joint #5 vs. pitch angle of blades during April 2022.

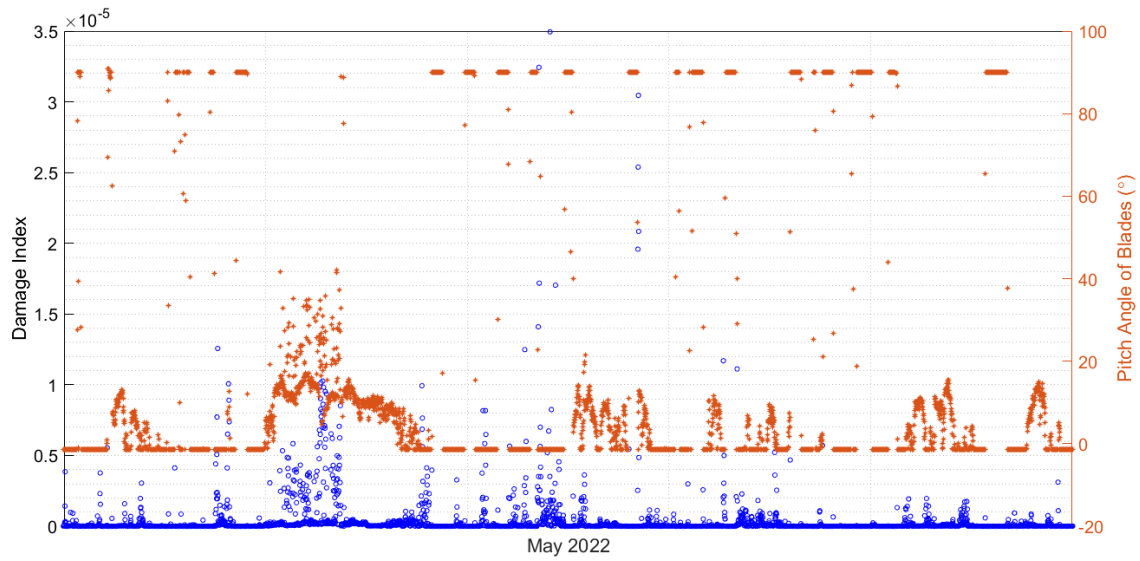


Figure 26. Damage index for the Jacket joint #5 vs. pitch angle of blades during May 2022.

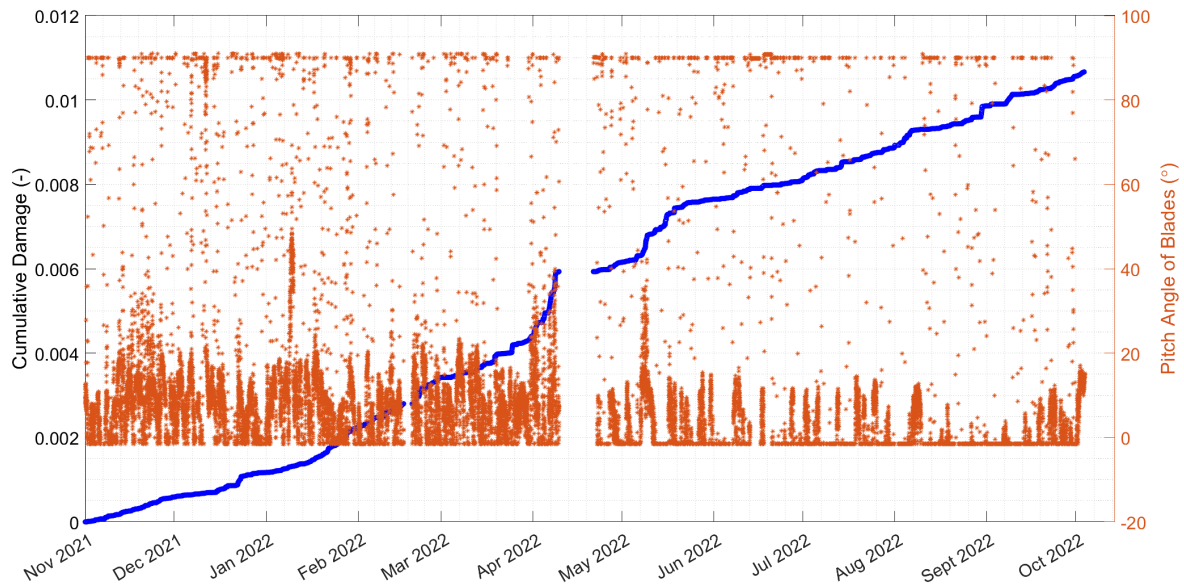


Figure 27. Cumulative damage of the Jacket joint #5 vs. pitch angle of blades during 1-year of monitoring from Nov. 2021 to October 2022.

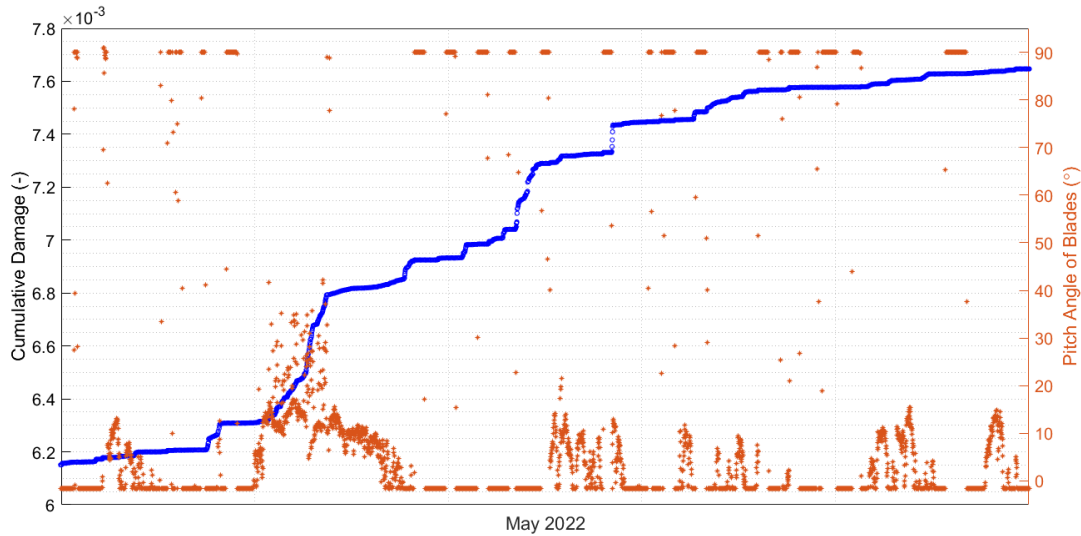


Figure 28. Cumulative damage of the Jacket joint #5 vs. pitch angle of blades during May 2022.

6 Conclusions

This report summarizes the structural fatigue behavior of Turbine B2 within the Block Island Wind Farm. The analysis of the tower fatigue yields the following observations:

- As expected, the fatigue of the tower at the points where the strain gauges were placed does not appear to drive the structural design. It is likely that other details near this section such as the flange or the bolted connection may be fatigue sensitive, but this was not under the scope of this report.
- The damage that did occur in the tower appeared to be related to pitch manipulation of the blades. However, the exact nature of the cause is difficult to tell without higher resolution SACADA information.
- There are two broad stress cycles that primarily damage the tower. There are cycles in the range from 10-30 MPa that appear to be related potentially to operational conditions. There is also damage from higher cycles above 30 MPa that appears to be related to unique events from turbine controls that cause large half cycle jumps.

Three critical joints in jacket structure are investigated during the 1-year monitoring period. The results of the analysis of the jacket nodes show that:

- The jacket legs are expected to experience a damage index of approximately 0.2 over a 25-year service life. Considering DFF of 3 for the jacket leg in seawater the leg joint in seawater is not expected to reach its allowable fatigue capacity within 25 years.
- Analysis of the leg joint in the splash zone shows the importance of corrosion protection for any fatigue design. If an in-air S-N curve is used, the allowable service life is estimated as 124 years and it experiences a damage index of about 0.2. Assuming that splash zone region is not inspectable and repairable and employing a DFF of 2, this joint would have an estimated service life of 62 years based on its allowable fatigue capacity.

- Fatigue design does not appear to be critical for the brace joint where damage accumulation remained low ($9E-6$) even over a projected 25-year service life.
- All jacket members have service lifetime greater than 20-year service life for which the B2 turbine is designed.
- The high damage indices in the jacket leg joints happened at two wind speed ranges: wind speed around 5 m/s where turbine starts to operate (startup condition); and wind speed around 10-11 m/s which turbine produces the maximum power, and the thrust is maximum.
- Another source for the high damage indices is the change of blades pitch angle which can be also considered as shut down/startup conditions. Several jumps in the cumulative damage plots of the jacket are due to the change of the blade pitch angle from 0 to 90 or the opposite.

7 Acknowledgments

This study has been completed as part of the Bureau of Safety and Environmental Enforcement (BSEE) project “Block Island wind farm structural monitoring project” under contract number 140E0119C0003. Additional support for this study has been provided by Massachusetts Clean Energy Center under the AmplifyMass program. The opinions, findings, and conclusions expressed in this document are those of the authors and do not necessarily represent the views of the sponsors and organizations involved in this project.

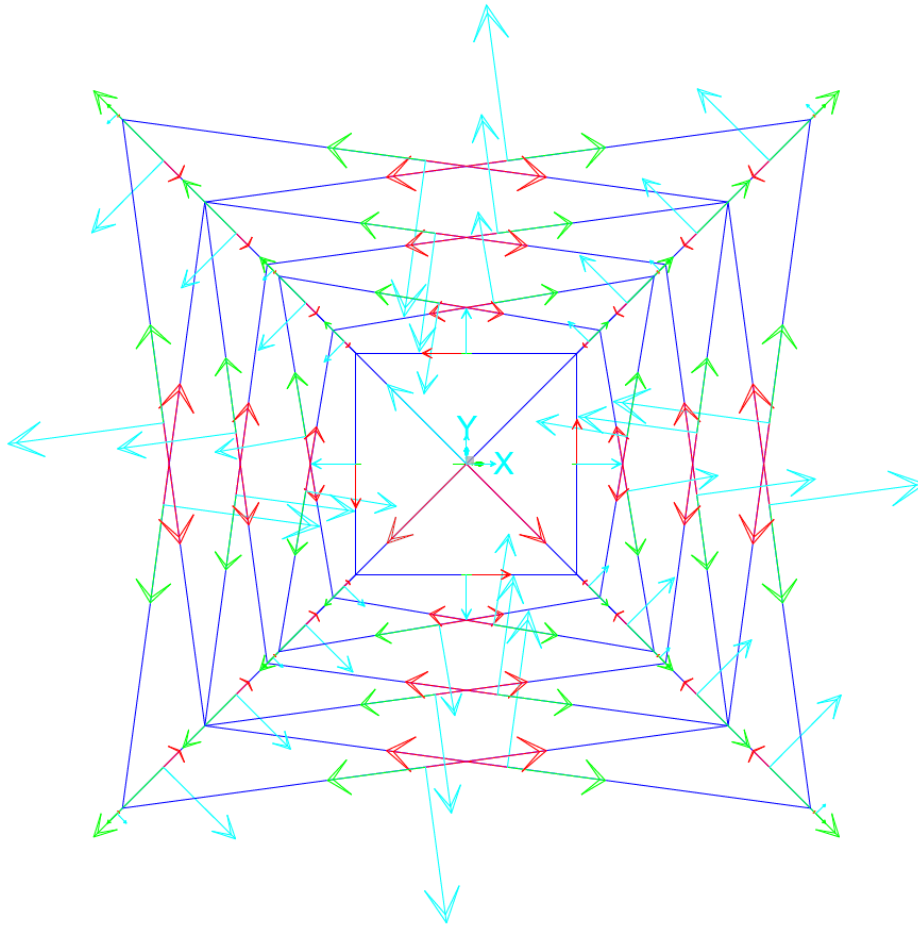
8 References

- ASTM-E1049-85. (2017). Standard Practices for Cycle Counting in Fatigue Analysis. In.
- Augustyn, D., Ulriksen, M. D., and Sørensen, J. D. (2021). Reliability Updating of Offshore Wind Substructures by Use of Digital Twin Information. *Energies*. 14(18), 5859.
- IEC (2019). IEC 61400-1: Wind energy generation systems - Part 1: Design requirements. *International Electrotechnical Commission*.
- Ding, L., Shun-Peng, Z., José, A. F. O. C., Abílio, M. P., Milan, V., and Filippo, B. (2022). Fatigue reliability of wind turbines: historical perspectives, recent developments and future prospects. *Renewable Energy*. 200: 724-742.
doi:<https://doi.org/10.1016/j.renene.2022.09.093>
- DNV. (2016). DNV-RP-0416-Corrosion protection for wind turbines. In (Edition 2016-03 - Amended 2021-10 ed.).
- DNV. (2021). DNV-ST-0126-Support structures for wind turbines. In.
- DNVGL-RP-C203. (2016). Fatigue design of offshore steel structures. In.
- Hines E., Baxter, C., Ciochetto, D., Song, M., Sparrevik, P., Meland, H.J., Strout, J.M., Bradshaw, A., Hu, S.L., Basurto, J.R., and Moaveni, B. (2023). Structural instrumentation and monitoring of the Block Island Offshore Wind Farm. *Renewable Energy*. 202: 1032-1045. January. <https://doi.org/10.1016/j.renene.2022.11.115>
- Joey, V., Claus, K., John Dalsgaard, S., and Gianluca, Z. (2020). Fatigue reliability of large monopiles for offshore wind turbines. *International Journal of Fatigue*, 134, 105487. doi:<https://doi.org/10.1016/j.ijfatigue.2020.105487>

- [Keystone. \(2015\). Deepwater Wind Block Island Wind Farm Sub-Structure and Foundation Design Report--Time Domain Fatigue Analysis. Doc. No. 5872A14-KEI-605-002. April.](#)
- MathWorks. Practical Introduction to Fatigue Analysis Using Rainflow Counting. Retrieved from https://www.mathworks.com/help/signal/ug/practical-introduction-to-fatigue-analysis-using-rainflow-counting.html#mw_rtc_PracticalIntroToFatigueAnalysisUsingRainflowCountingExample_M_68F0E3B8
- Ørsted. (2016). Block Island Wind Farm. Retrieved from https://us.orsted.com/wind-projects?gclid=Cj0KCQjwnoqLBhD4ARIsAL5JedICXBeoZ3HcdIB6Tm15iQZ7y2v3F6jhkpsMa1v7Ftwqv1LBDbHKBQAaAmTcEALw_wcB
- Pacheco, J., Pimenta, F., Pereira, S., Cunha, Á., and Magalhães, F. (2022). Fatigue assessment of wind turbine towers: Review of processing strategies with illustrative case study. *Energies*. 15(13), 4782.
- Renqiang, X., Xiuli, D., Piguang, W., Chengshun, X., Endi, Z., and Suyu, W. (2021). Dynamic analysis of 10 MW monopile supported offshore wind turbine based on fully coupled model. *Ocean Engineering*. 234. 109346.
doi:<https://doi.org/10.1016/j.oceaneng.2021.109346>

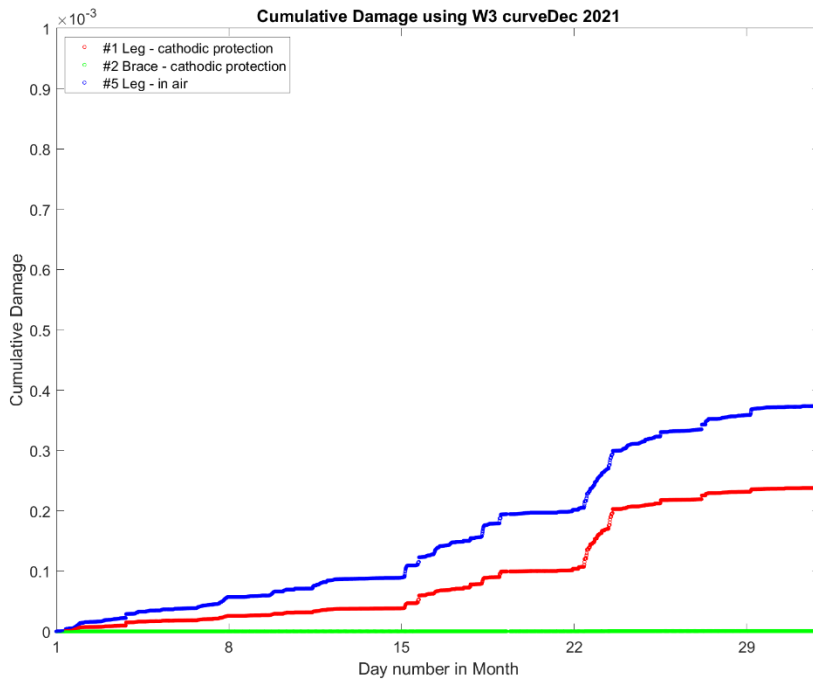
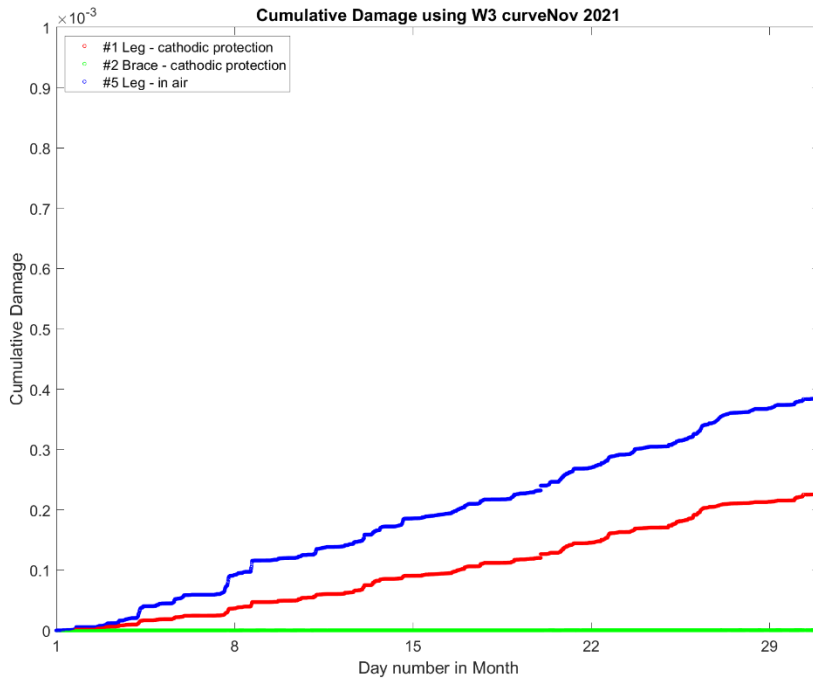
Appendix A

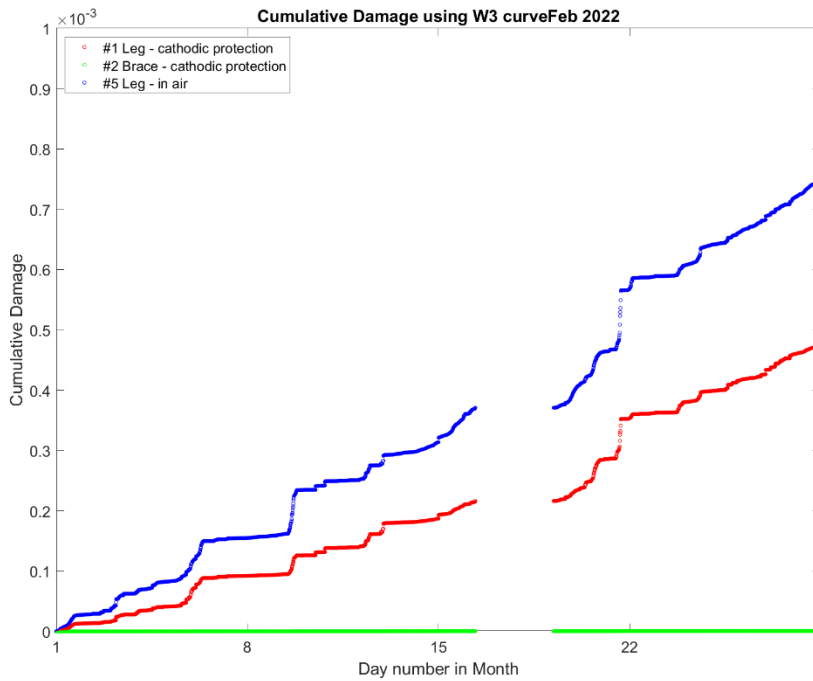
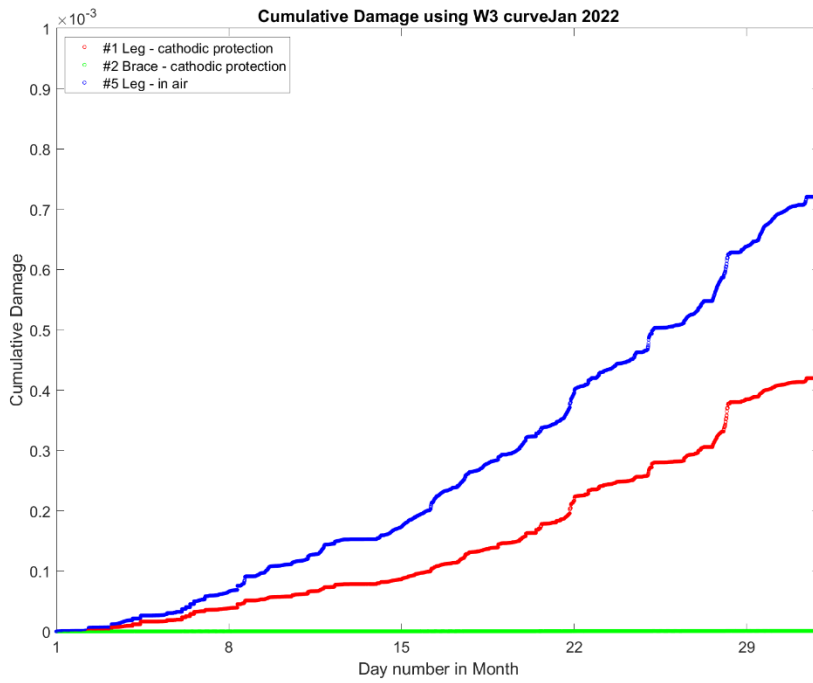
The following plot shows the local axes 2 (green) and 3 (blue) on all elements of the BIWF-B2 jacket foundation in the SAP2000 FE model.

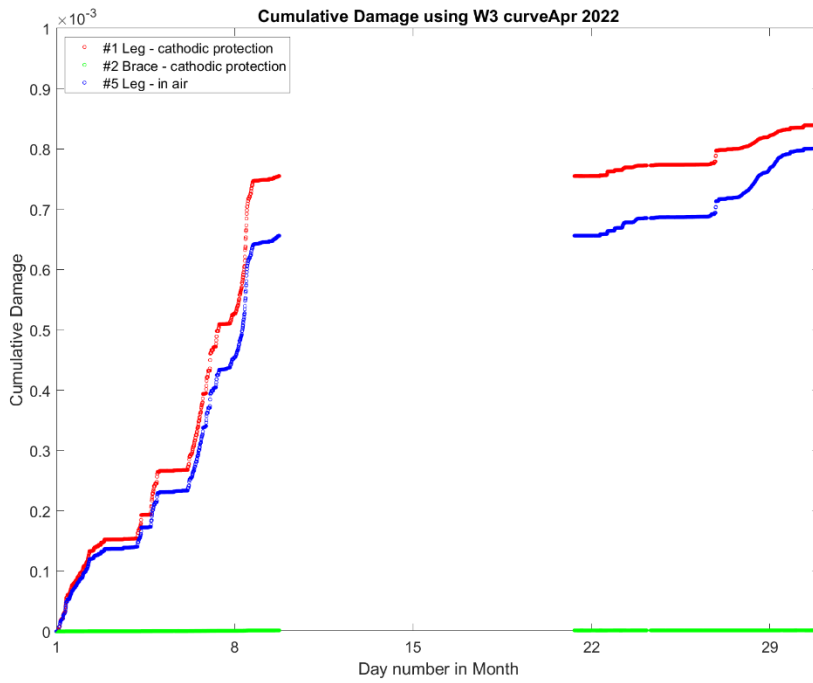
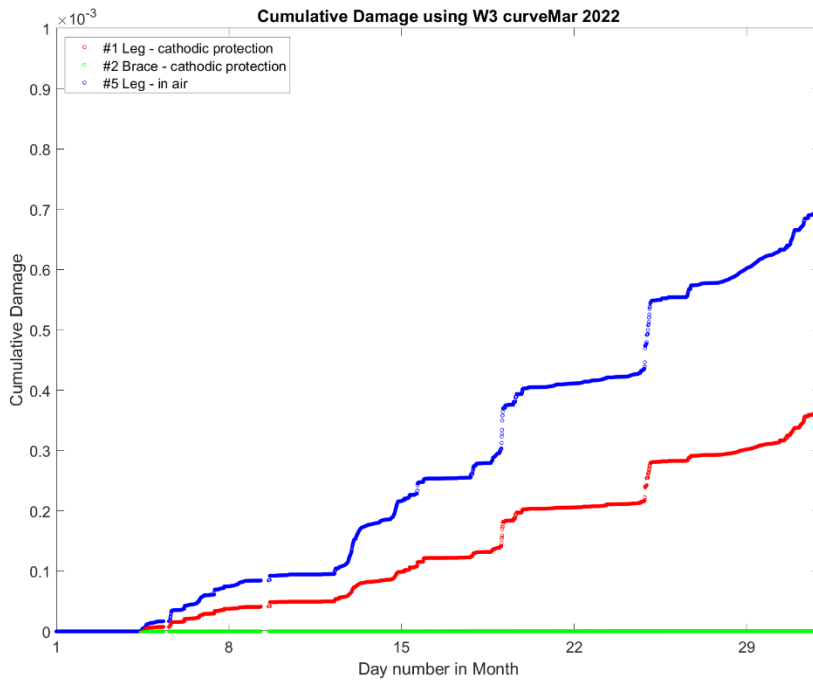


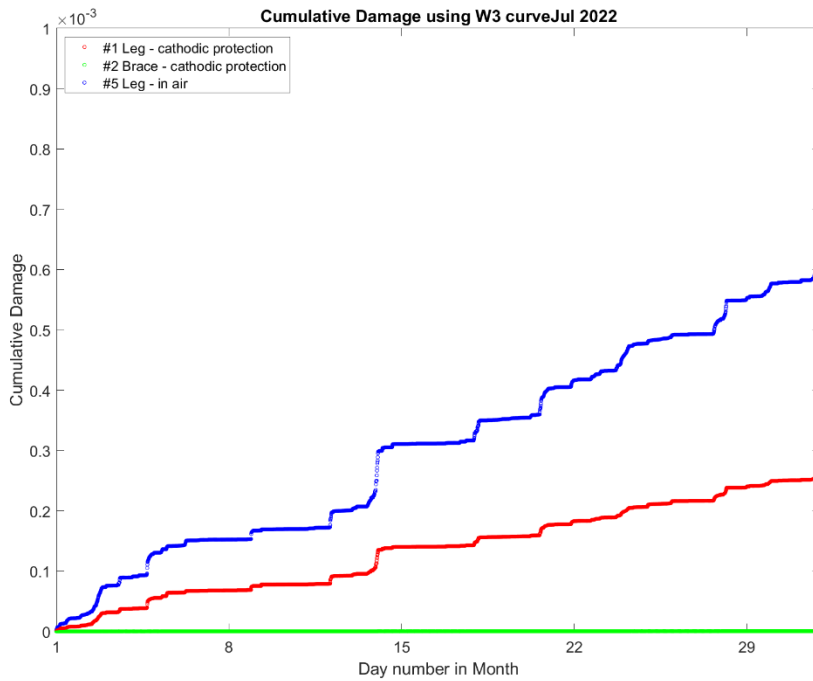
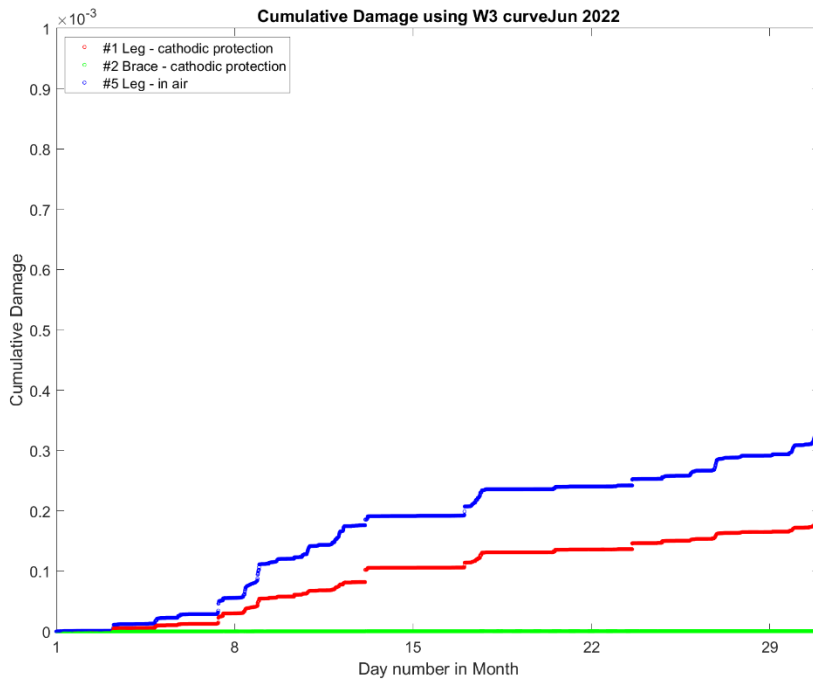
Appendix B

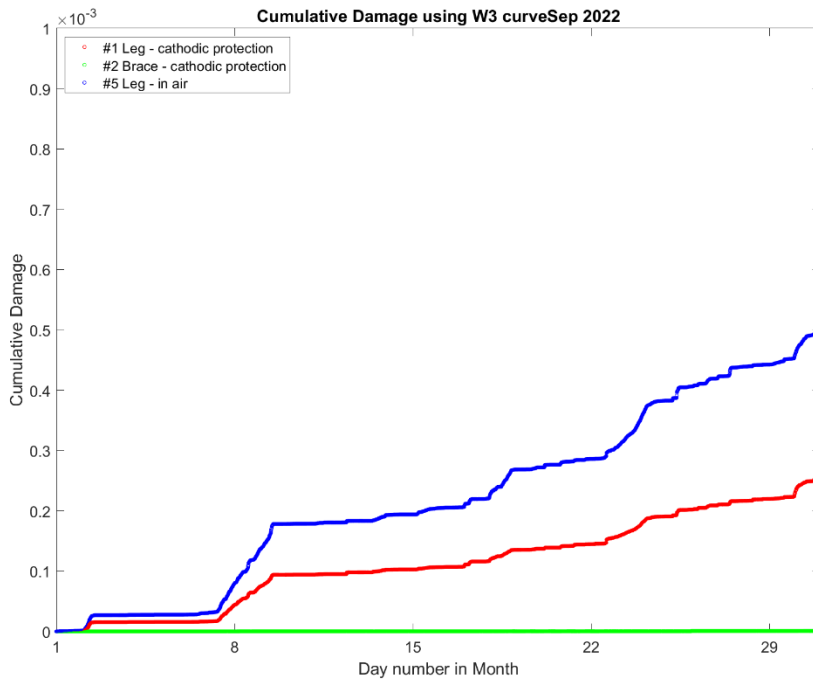
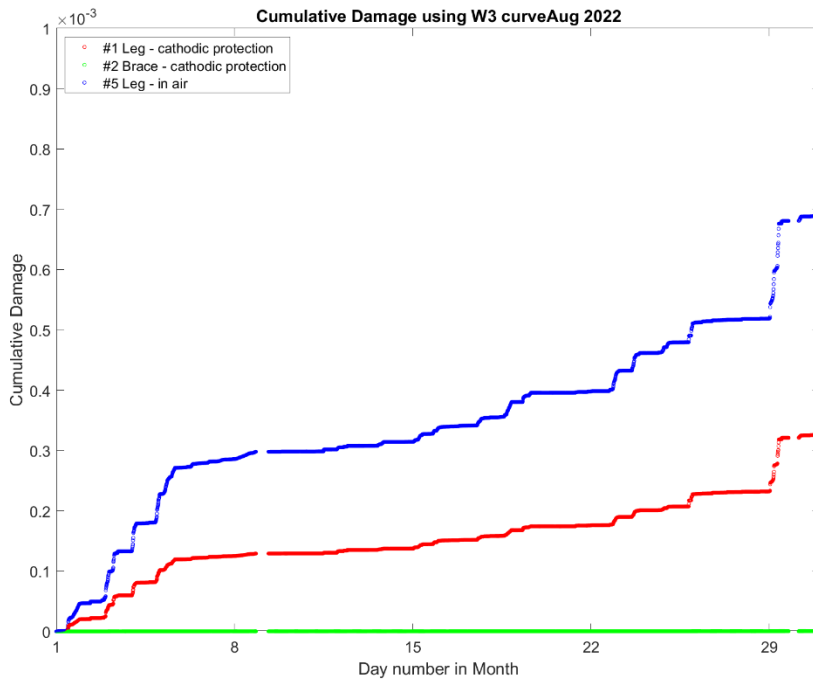
In this appendix, we provide the cumulative damages of the jacket joints for months from Nov. 2021 to September 2022 except for May 2022.





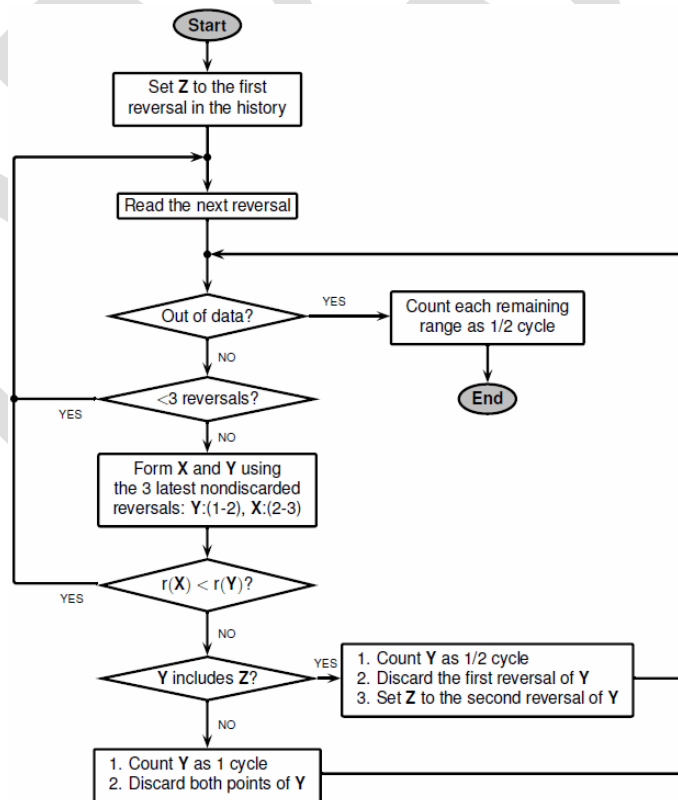
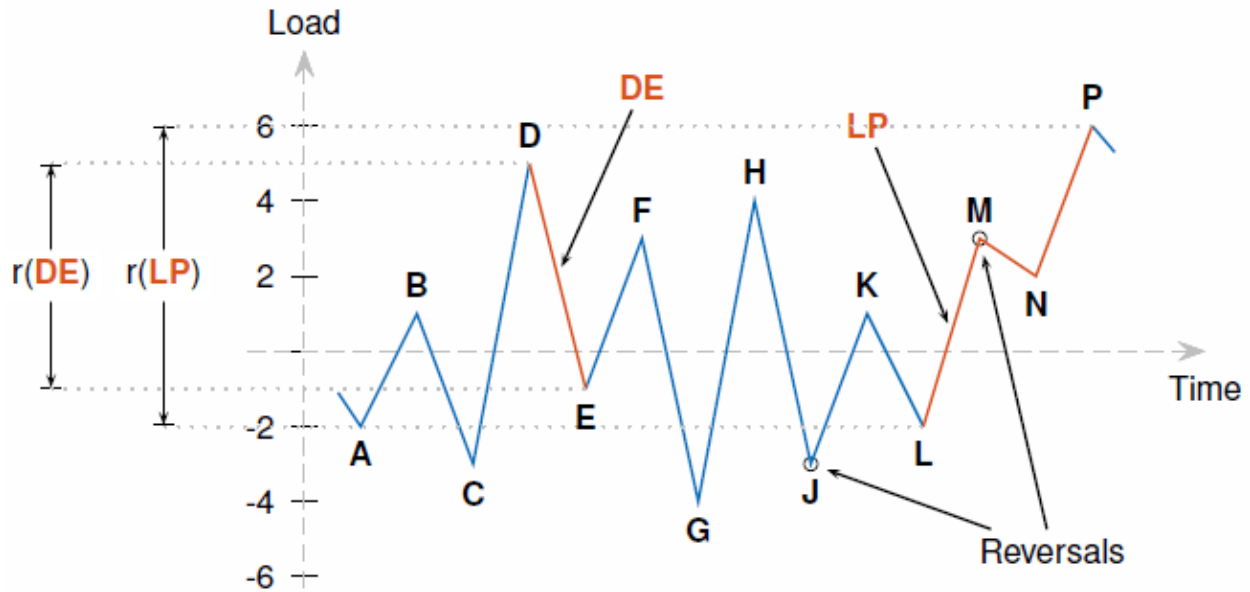






Appendix C

In this appendix we provide an overview of how rainflow counting works. This overview comes from the Matlab documentation at the following link: [Rainflow counts for fatigue analysis - MATLAB rainflow \(mathworks.com\)](https://www.mathworks.com/help/matlab/rainflow.html). Below is an example of a possible signal followed by the flowchart from Figure 3. This appendix will walkthrough the process of how the algorithm counts.



The algorithm begins by looking at the first three points ABC and A is set as the starting point Z. Following the algorithm Y is defined as the distance from A-B, $r(Y) = 3$, and X is defined as the distance from B-C, $r(X) = 4$. Because $r(X) = 4$ is GREATER than $r(Y) = 3$ and our Y points AB include the starting point Z the algorithm counts Y as a $\frac{1}{2}$ cycle and moves point Z to point B.

The algorithm then adds point D to look at BCD with the starting point Z set at point B. BC is set to Y and $r(Y) = 4$ while CD is set to X and $r(X) = 8$. The same check is done with $r(Y)$ and $r(X)$ and the same result occurs as the last check so BC is counted as a half cycle and the algorithm moves on to CDE.

For CDE the $r(Y) = 8$ and $r(X) = 4$. Because $r(X)$ is LESSER than $r(Y)$ the algorithm now does something different than it did for the past two checks. Now the next point is read to look at CDEF where point Z is still defined as C. In this loop Y is set to DE and X is set to EF with $r(Y) = 6$ and $r(X) = 4$. Because $r(X)$ is still LESSER than $r(Y)$ the algorithm again reads the next point, G.

For CDEFG Y is set to EF and X is set to FG. In this case $r(X) = 4$ is GEATER than $r(Y) = 7$. As a result, the algorithm does not move on to read the next point. Also, because no points in Y, EF, include the Z point, C, no half cycle is recorded. Instead, EF is recorded as 1 full cycle.

After counting 1 cycle the algorithm then throws out the two EF points which leaves CDG. This makes CD the Y and DG the X. Because $r(X) = 9$ is GREATER than $r(Y) = 8$ the algorithm does not read the next point and instead counts Y as a half cycle and moves the starting point, C, again. This process continues for all points. The table below was taken from the MATLAB link.

| Step | Z | Reversals | Three Reversals? | Y | r(Y) | X | r(X) | $r(X) < r(Y)$? | Z in Y? | Actions |
|------|---|---------------------|------------------|----|------|----|------|-----------------|---------|--|
| 1 | A | A, B, C | Yes | AB | 3 | BC | 4 | No | Yes | 1. Count AB as $\frac{1}{2}$ cycle. 2. Discard A. 3. Set Z to B. |
| 2 | B | B, C | No | - | - | - | - | - | - | Read D. |
| 3 | B | B, C, D | Yes | BC | 4 | CD | 8 | No | Yes | 1. Count BC as $\frac{1}{2}$ cycle. 2. Discard B. 3. Set Z to C. |
| 4 | C | C, D | No | - | - | - | - | - | - | Read E. |
| 5 | C | C, D, E | Yes | CD | 8 | DE | 6 | Yes | - | Read F. |
| 6 | C | C, D, E, F | Yes | DE | 6 | EF | 4 | Yes | - | Read G. |
| 7 | C | C, D, E, F, G | Yes | EF | 4 | FG | 7 | No | No | 1. Count EF as 1 cycle. 2. Discard E and F. |
| 8 | C | C, D, G | Yes | CD | 8 | DG | 9 | No | Yes | 1. Count CD as $\frac{1}{2}$ cycle. 2. Discard C. 3. Set Z to D. |
| 9 | D | D, G | No | - | - | - | - | - | - | Read H. |
| 10 | D | D, G, H | Yes | DG | 9 | GH | 8 | Yes | - | Read J. |
| 11 | D | D, G, H, J | Yes | GH | 8 | HJ | 7 | Yes | - | Read K. |
| 12 | D | D, G, H, J, K | Yes | HJ | 7 | JK | 4 | Yes | - | Read L. |
| 13 | D | D, G, H, J, K, L | Yes | JK | 4 | KL | 3 | Yes | - | Read M. |
| 14 | D | D, G, H, J, K, L, M | Yes | KL | 3 | LM | 5 | No | No | 1. Count KL as 1 cycle. 2. Discard K and L. |
| 15 | D | D, G, H, J, M | Yes | HJ | 7 | JM | 5 | Yes | - | Read N. |
| 16 | D | D, G, H, J, M, N | Yes | JM | 5 | MN | 1 | Yes | - | Read P. |
| 17 | D | D, G, H, J, M, N, P | Yes | MN | 1 | NP | 4 | No | No | 1. Count MN as 1 cycle. 2. Discard M and N. |

In summary, there are 3 decisions the rainflow cycle algorithm may make. First, count a half cycle and move the starting point, Z. Second, count a full cycle and remove both points from the points of interest. Third, count no cycles and just read the next point. What the algorithm does is dependent on the relationship between two neighboring half cycles defined as Y and X.